The effects of posture on the position and shape of abdominal and thoracic organs

Philippe Beillas, Yoann Lafon, Francis Smith

Stapp Car Crash Journal, Vol. 53 (November 2009), pp.

The Effects of Posture and Subject-to-Subject Variations on the Position, Shape and Volume of Abdominal and Thoracic Organs

Philippe Beillas and Yoann Lafon
Université de Lyon, F-69622, Lyon, France;
INRETS, UMR_T9406, LBMC, Université Lyon 1.

Francis W. Smith
Positional MRI Center, University of Aberdeen, Aberdeen, Scotland

ABSTRACT – In this study, the thorax and the abdomen of nine subjects were imaged in four postures using a positional MRI scanner. The four postures were seated, standing, forward-flexed and supine. They were selected to represent car occupants, pedestrians, cyclists and a typical position for medical imaging, respectively. Geometrical models of key anatomical structures were registered from the imaging dataset using a custom registration toolbox. The analysis of the images and models allowed the quantification of the respective effects of posture and subject-to-subject variation on the position, shape and volume of the abdominal organs, skeletal components and thoracic cavity. In summary, except for the supine posture, the organ volumes and their positions in the spinal frame were mostly unaffected by the posture. The supine posture was associated with a motion of all solid organs of up to 39 mm (interpostural maximum for the liver, n=9), and a reduction of the thoracic cavity volume of up to 1300 cm^3. Subject-to-subject variations were especially large for the volume of the spleen (variations between 120 and 400 cm^3) and the position of the kidneys. As a result, subject-to-subject variations were larger than most postural effects. Other results include values of parameters that can help positioning human models such as positions, volumes and inertial properties of organs as well as skeletal parameters. Overall, this study suggests that subject-to-subject variations and the use of supine geometrical data can be problematic for finite element modeling of the abdomen for injury prediction.

KEYWORDS – MRI, abdomen, organ, liver, kidney, spleen, geometry, registration, posture, inertia, volume, organ, pedestrian, occupant, cyclist, supine

INTRODUCTION

Postural changes, from lying supine to sitting in a car, standing like a pedestrian or leaning forward when riding a bicycle, affect the position of bones and soft tissues. These postural changes may also affect the position and shape of internal organs, especially in a very soft region such as the abdomen.

Experimental approaches to study the size and position of internal anatomical structures have included the use of X-Ray, CT-scan, fluoroscopy, MRI and ultrasound (Langen and Jones, 2001). Using those techniques, numerous authors have studied the motion of an organ associated with breathing, often because it can affect the accuracy of treatment delivery. Recently, Brandner et al. (2006) tracked the motion of all solid organs in a population of 13 subjects during normal breathing in a supine position using 4D CT. They found amplitudes of motion between 11 and 13 mm depending on the organ. This is in agreement with other studies on specific organs (Langen and Jones, 2001). The position of the diaphragm was also quantified as a function of the posture and breathing strategy. For example, Wade (1954) found that, when going from supine to standing, the average distances between the iliac crest and the leaves of the diaphragm varied by approximately 38 mm and 29 mm for the right and left leaves of the diaphragm, respectively.

Recently, MRI techniques have been used to quantify the change of shape of an organ during breathing (e.g. liver in Rohlfing et al., 2004), organ filling (e.g. bladder in Lotz et al., 2005), or muscle relaxation (e.g. colon in Frøkjaer et al., 2007). However, these studies were limited to one organ or one posture. This is also the case for the three-dimensional geometrical datasets that were used for the development of various finite element (FE) models of road users (e.g.

Address correspondence to Philippe Beillas. Electronic mail: philippe.beillas@inrets.fr

HUMOS, H-Model, THUMS). These three-dimensional datasets were generally derived from a single subject, using either destructive slicing of a single post mortem human subject lying supine or seated (e.g. datasets from the Visible Human Project or the HUMOS Project) or medical imaging obtained in supine posture (MRI, CT). More recently, Bertrand et al. (2006) collected geometrical data in seated and standing postures on a population of over sixty volunteers using low dose X-ray imaging. However, the results only included skeletal parameters.

While large amounts of literature are available on organ motion, there does not seem to be three-dimensional organ data available in multiple postures, including postures typically observed for road users (e.g. seated). The absence of such data makes it difficult to accurately position the organs of finite element models in different road user positions. Furthermore, the accurate knowledge of organ positions would be important if injury prediction was attempted based on strain or stress calculation, because they would have little meaning if the organ location were incorrect.

Therefore, the aims of the current study were to quantify the effects of posture on the position and shape of the main anatomical structures of the abdomen and thorax, and compare them with the effects of subject-to-subject variations. The study included both soft organs and skeletal structures, and covered the regions from the pelvis to the upper thoracic vertebra T1.

METHODS

An MRI based method was developed to quantify the effects of posture on the position and shape of the abdominal organs. The postures included one reference posture (supine) and postures typically observed for three categories of road users: pedestrian, vehicle occupant and cyclist (standing, seated and forward-flexed, respectively). Nine subjects were used in the current study. Their key characteristics are provided Table 1. All imaging was performed at the Positional MRI Center of the University of Aberdeen (Aberdeen, Scotland)*. The subjects had no known pathology and were screened for possible contraindication with MRI scanning.

Table 1: Key characteristics for the nine subjects used in the current study.

Number	Sex	Height (m)	Weight (kg)	BMI	Age (y)
M01	Male	1.75	70	22.9	29
M02	Male	1.91	88	24.1	32
M03	Male	1.75	64	20.9	29
M04	Male	1.69	60	21.0	26
M05	Male	1.81	80	24.4	26
M06	Male	1.83	82	24.5	37
F01	Female	1.74	68	22.5	41
F02	Female	1.72	64	21.6	42
F03	Female	1.62	53	20.2	34

Imaging

All imaging was performed using a Fonar Upright MRI scanner (Melville, NY). Due to the limited field of view, abdominal and thoracic imaging were performed in separate acquisitions with an overlap to facilitate the registration. Abdominal acquisitions spanned from a minimum of 3 to 5 cm above the diaphragm to at least part of the femoral heads. Thoracic acquisitions spanned from a minimum of 3 to 5 cm below the diaphragm to the spine at least up to the C7 vertebra. Specific imaging of the pelvis was also necessary, as the most distal parts of the pelvis were not visible in the abdominal acquisitions. Pelvic imaging was only performed in the seated posture for most subjects because the pelvis can be considered as rigid under gravity loading. For each subject, the imaging was performed in a single period of less than four hours and each acquisition lasted around 3 minutes.

The main acquisitions were performed in a sagittal plane using a fast spin echo T1 sequence. The slice resolution was 256 by 256 pixels, with a pixel size of 1.5625 mm by 1.5625 mm, leading to a 400 mm by 400 mm imaging area. The slice thickness was always 5 mm but the number of slices or the gap (up to 1 mm) were adjusted to image the complete width of the subject. This lead to 54 to 60 slices depending on the width of the subject. The MRI was not gated and the subjects were instructed to breathe quietly during the acquisition. This approach provides a better cycle-to-cycle repeatability than a breath hold approach (Blackall et al., 2006). When time permitted, coronal imaging was also performed to provide a second viewpoint for the identification of structures.

*The imaging protocol used in this study was authorized by a properly constituted ethics committee at the imaging site (University of Aberdeen, Scotland).

Posture definition and implementation

For image quality purposes, the region of interest and the imaging coil needed to be positioned at the center of the magnet. Positioning was achieved using a combination of MRI table motion and custom-designed adjustable fixtures. The four postures are described hereafter and illustrated on Figure 1.

Supine (reference). The table was set in its horizontal position and the subject was lying supine on top of it. A quadratic rigid coil was used for this imaging.

Standing (pedestrian). The table was set to its most vertical position (5-degrees tilt towards the back of the machine) and the subject was standing with his/her back against the table. The quadratic coil was also used for this imaging.

Seated (occupant). The subject was seated in a custom built seat that could be mounted on the table. A seat back angle of 25 degrees with the vertical was selected to represent a typical seat back angle. This seat back angle was obtained by a 15 degrees table tilt and an additional 10-degree seat back. The seat pan angle with the horizontal plane was 9 degrees. The seat was height adjustable. A soft coil was used for this imaging.

Forward-flexed (cyclist). Cyclists positions appear to vary widely with biking practices. While the torso can be almost vertical for some city usage (e.g. "Dutch" bike), it is almost horizontal for cyclists involved in track competitions. Since no standard posture was found in the literature, an intermediate back angle of 45 degrees was selected arbitrarily for the current study. This corresponds to the intermediate posture used in a previous study by Gemery et al. (2007). No bicycle-like fixture was used due to space limitation issues and also because remaining completely immobile on such a fixture during several minutes could be difficult or uncomfortable (forces on the hands, wrists, elbow and seat pressure). Therefore, the subject was positioned using the following procedure: first, the table was angled at 15 degrees from the vertical. Then the subject stood against the table and flexed forward while keeping the pelvis in contact with the table. A foam angle was inserted between the table and the back of the subject to facilitate the positioning at 45 degrees. The foam was removed before the imaging. An elbow plate, a head chiropractic cushion, and knee/thigh fixtures supported the subject as illustrated on Figure 1. When needed, the subject's vertical position with respect to the magnet was adjusted using a small step under the feet or by using a knee-flexed position. A soft coil was used for this imaging.

In all four postures, the arms were at approximately 90 degrees from the torso. Transverse bars were blocked between the sides of the magnet to serve as supports when needed (Versa Rest in Fonar terminology). All additional fixtures and supports were custom-built using MRI compatible materials.

Data processing

The data were processed using a custom toolbox, the Imod (University of Colorado, Boulder) and Scilab (www.scilab.org) open-source software packages. The toolbox linked the two packages. It was developed specifically to perform the registration and the data analysis. A description of the overall process follows.

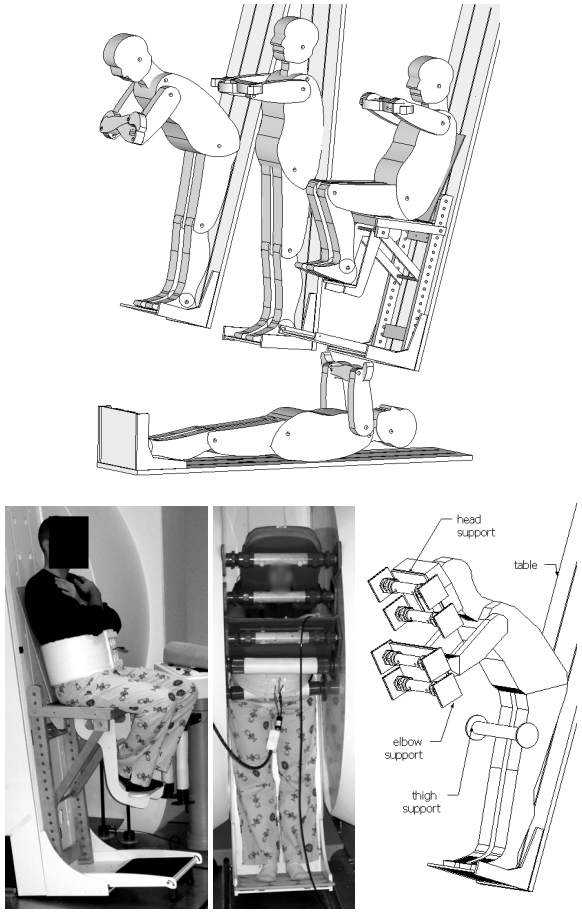

Figure 1: Postures used in the Fonar Upright MRI. Top: summary of the four postures (forward-flexed, standing, seated and supine). Bottom left: picture of the seated posture, outside of the magnet. Bottom center: anterior picture of the forward-flexed posture inside the magnet. Bottom right: schematics of the forward-flexed posture with the head, elbow and thigh supports (the magnet is not shown).

First, overlapping image datasets were registered manually using a rigid registration scheme. The initial positioning of the datasets was facilitated by the use of Beekley MR-Spots 185 skin markers (Bristol, CT). When differences could be observed in the overlapping region of adjacent scans due to small organ motion, the abdominal scan was always used as the reference.

Then, an interactive model-based approach was used for the registration. First, a reference model based on the Visible Human Male dataset (National Library of Medicine, Bethesda, MD) was deformed to match the seated imaging dataset. The deformation process consisted in successive geometrical transformations of the model. Each transformation could be rigid, affine or non-linear (Trochu, 1993). The operator defined the transformation parameters by selecting control points on the model and images or by direct numeric input. The resulting model was selected as the new reference. Then, the interactive deformation process was repeated for the three other postures. The models included several objects that could be deformed individually or in groups. These objects were three-dimensional polygonal surface meshes representing the following anatomical structures:

- *Skeletal structures:* vertebrae from C7 to L5 (spine object), pelvis, sternum, femoral heads. Each object had associated landmarks for the post-processing.
- *Solid organs:* liver, spleen and kidneys.
- Skin.
- A thoracic cavity object composed of lungs, heart, esophagus, trachea and large thoracic vessels up to the level of T1.
- An object including liver, spleen, stomach, intestines, pancreas and mesentery. The object did not include the kidneys, the uterus nor the rectum. It is very similar to the peritoneal cavity. The main difference is that it included the duodenum and the pancreas. This object was called the "abdominal object".

The ribs, the pancreas and the components of the digestive systems were not described individually because their definition was difficult or too time consuming. The pelvis was assumed as rigid. Its registration was based on the regions above the femoral heads when it was not imaged in its entirety. The spine registration was solely based on the vertebral bodies and no attempt was made to match the position of the posterior elements.

The registration process resulted in one three-dimensional model per subject per posture. The results were expressed in a spinal frame defined by Stokes (1994) as follows: the origin is at the center of the sacral plate S1, Z is the axis between S1 and the center of T1 vertebra, X0 (postero-anterior) results from the cross product between Z and the axis passing though the acetabular cups and Y results from the cross product of Z and X0. The position of the spinal frame was computed in a global (or laboratory) frame, where Z_G is vertical, Y_G is the axis of the magnet and X_G is horizontal towards the front of the machine.

The following parameters were defined to compare the models:

- Spinal length: the length of a spline passing though the landmarks at the center of the vertebral bodies from T1 to L5.
- Lordosis and kyphosis angles (between T4-T12 and L1-L5, respectively). They were computed from the spline passing through the landmarks at the center of the vertebral bodies as described in Appendix A.
- Pelvic tilt: angle between the Z-axis of the spinal frame and the line going through the centers of S1 and the femoral heads (projected in a mid sagittal plane). A description of the pelvic tilt is provided in Appendix A Figure A-2.
- Angle $\theta 1$ between the X-axis in the global frame and the line passing through the center of the sacral plate and the anterior superior iliac spine of the pelvis (as defined in Leung et al., 1979). A description of the angle is also provided in Appendix A Figure A-3.
- The angle between the sternum and T4-T10, and the distance between the center of the sternum and T7.
- The position of the upper point of the diaphragm in the spinal frame along the Z-axis
- The L4-to-skin distance: computed from the center of L4 to the intersection of the skin on the anterior abdominal surface and a line passing through L4 parallel to the X-axis (spinal frame).
- Inertial properties: position of the center of gravity, volume and inertial moments were computed using a method published by Mirtich (1996). This method is based on the reduction of the volume integrals to simpler integrals using the divergence theorem and Green's theorem.

- Mesh-to-mesh bilateral distances between objects were computed and plotted using the MESH software package (Aspert et al., 2002).

All parameters were computed using the custom toolbox except for the mesh-to-mesh distance. To illustrate the differences of shapes, models were positioned using an Iterative Closest Point method (ICP) in the Meshlab software (Visual Computing Lab, ISTI, CNR, http://meshlab.sourceforge.net/).

Since the skin object extended beyond the boundaries of the imaged region, its inertial properties were only based on the volume contained between a plane perpendicular to the S1-T1 axis at T1 and a plane passing through S1 making an angle of 50 degrees with the axis passing through S1 and the pubic symphysis. An illustration of the objects, planes and spinal frame is provided in Figure 2.

The Wilcoxon two-sided signed-rank test was used to identify significant effects. The tests were performed by comparing the value of a parameter in two postures, or the variations of this parameter between any two postures. A P-value <0.05 was considered as significant. The test was computed using the Stixbox statistical toolbox. Results from the current study were also compared with literature data when available.

A basic evaluation of the approach used in the toolbox was performed by comparing results obtained from a manual segmentation of the high resolution images of the Visible Human Female Dataset with outputs from the toolbox applied to the same images after downsampling. For a 1 mm voxel (volumetric pixel) size, the volume differences for the spleen, kidneys and liver were less than 0.4%, and the object-to-object distances were less than 1.6 mm for 95% of the samples. For the 5 mm voxel size, the differences were 11.2% and 4.4 mm, respectively.

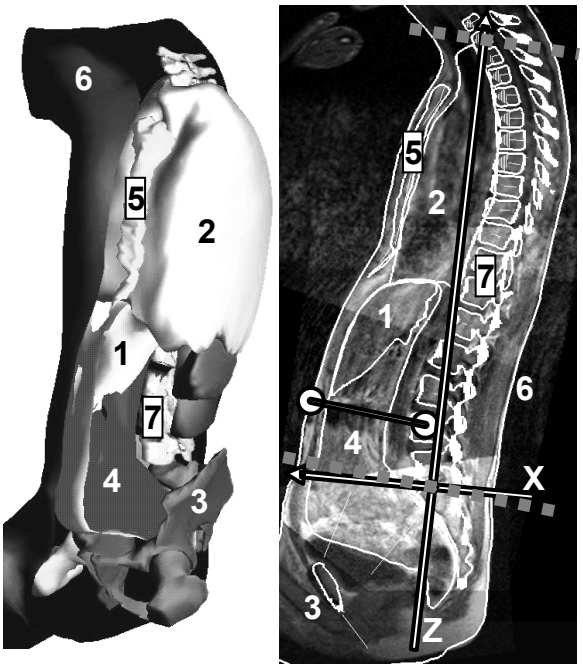

Figure 2: Objects defined in the current study. Left: model view (Skin and abdominal object partially shown). Right: intersection between a registered model and a sagittal section. The arrows illustrate the position of the spinal frame (X-axis and Z-axis). The objects that are labelled in this illustration are: (1) Liver; (2) Thoracic object; (3) Pelvis; (4) Abdominal object; (5) Sternum; (6) Skin; (7) Spine. The dotted lines illustrate the approximate positions of the planes used to bound the skin for the volume computation. The line terminated by small circles corresponds to the L4-to-skin distance.

RESULTS

The abdominal and thoracic scans corresponding to the 36 positions (9 subjects, 4 postures) were performed successfully. The only exception was the case of subject M02, who was too tall for the thorax imaging in the forward-flexed posture. The data processing (image and model registration) was performed successfully on all available scans. An illustration of the nine subjects in four postures with their corresponding models is provided in Figure 3. Qualitatively, some of the postural effects (e.g. depth of the abdomen in supine vs. other postures) can be observed in Figure 3.

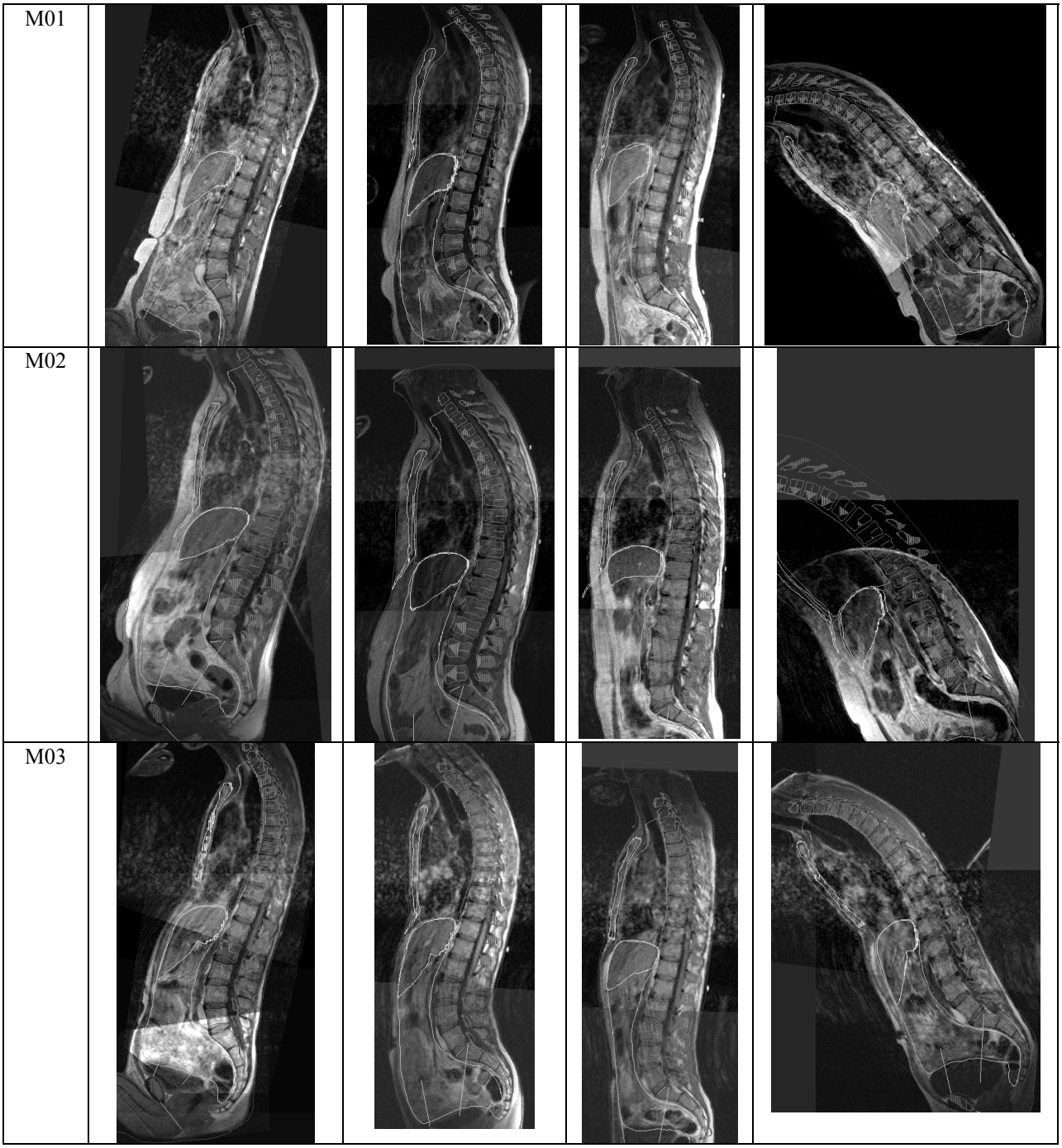

Figure 3: Mid-sagittal sections (imaging and model) in all four postures (from left to right: seated, standing, supine and forward-flexed) for the nine subjects. The orientation of the image is provided on the last line of the table.

Figure continued on next page.

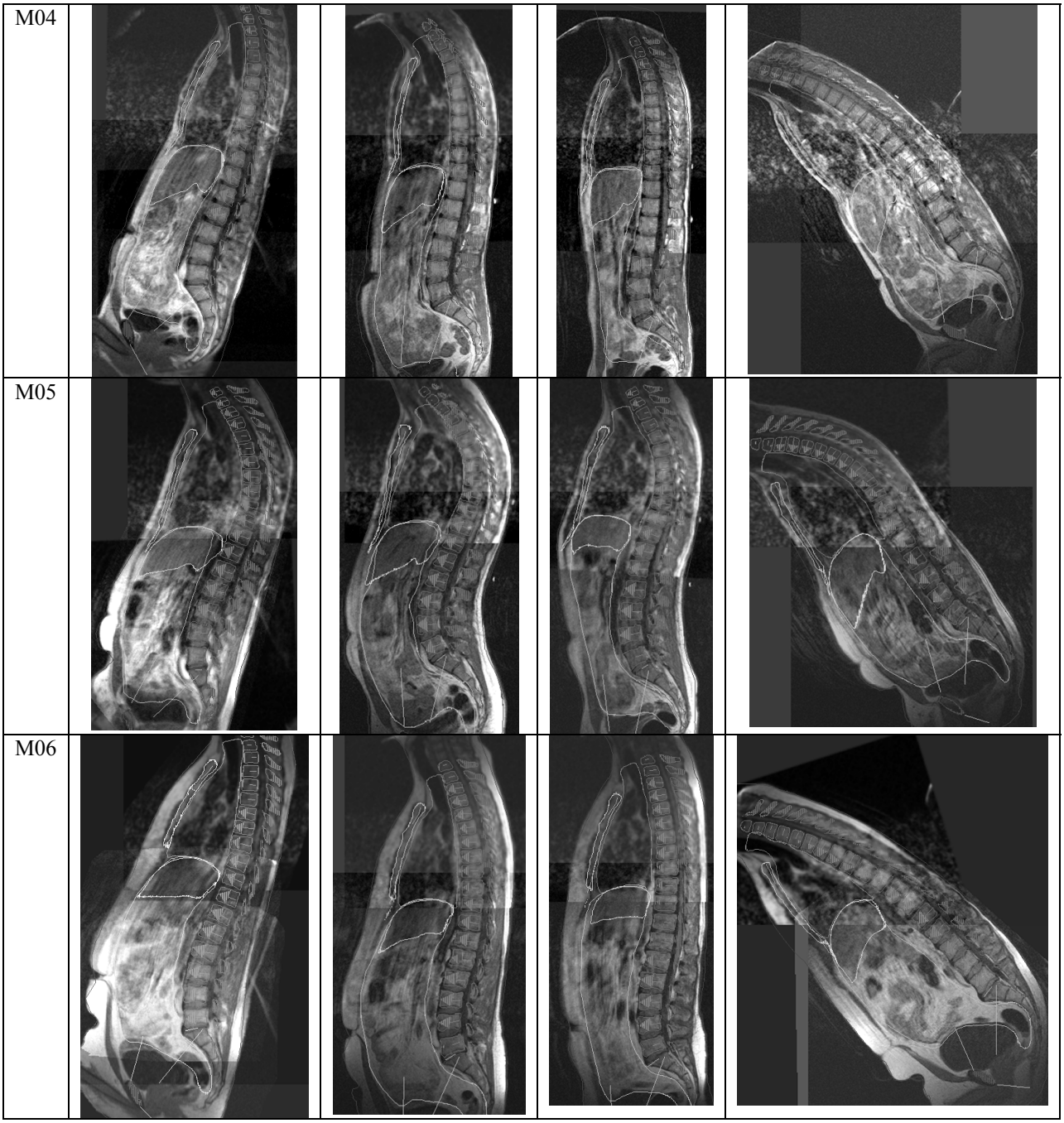

Figure 3: Mid-sagittal sections (imaging and model) in all four postures (from left to right: seated, standing, supine and forward-flexed) for the nine subjects. The orientation of the image is provided on the last line of the table.

Figure continued on next page.

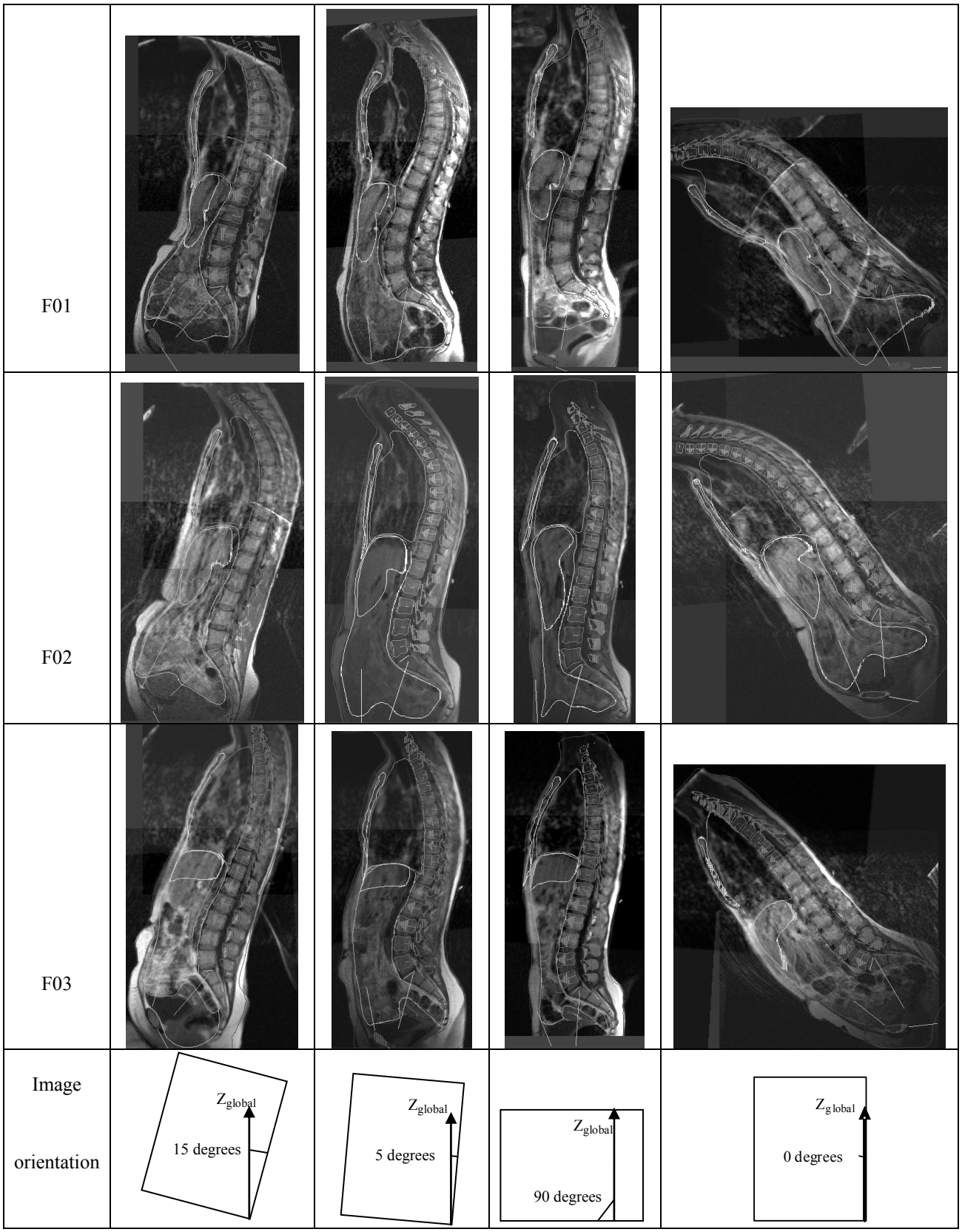

Figure 3: Mid-sagittal sections (imaging and model) in all four postures (from left to right: seated, standing, supine and forward-flexed) for the nine subjects. The orientation of the image is provided on the last line of the table.

Overall position and bony parameters

In the forward-flexed posture, the angle of the S1-T1 axis with the vertical direction varied between 41 and 56 degrees, with a standard deviation of 5 degrees (Table 2). The standard variations were smaller in the three other postures (3 degrees or less).

For all subjects, the spinal length between T1 and L5 varied by less than 3% of the average length (13 mm at most, Table 3), and none of the differences between any two postures were statistically significant ($p>0.1$). For the other spinal parameters, the kyphosis, lordosis and pelvic tilt angles varied with the posture in a fairly repeatable pattern among the subjects (Figure 4). The relationship between subject-to-subject variability and the effects of posture is illustrated in Figure 5. The posture also affected the angle θ1, with average angles between 13 and 66 degrees depending on the posture (Table 4). The supine angle was 66 degrees with respect to the vertical, or 24 degrees with respect to the horizontal, which is similar to the standing value of 22 degrees. The spinal parameters were significantly different between any two postures ($p<0.027$) with the exceptions of the seated vs. forward-flexed and the kyphosis in standing vs. forward-flexed. However, subject-to-subject variations of kyphosis angle were of similar magnitude as the effect of posture, while the effect of posture was more predominant for the lordosis and pelvic tilt. The values of kyphosis, lordosis, pelvic tilt and angle θ1 were similar to literature in comparable postures (Table 6).

The position of the center of the sternum with respect to the thoracic spine (distance between sternum center and T7, angle between T4-T10 and T7-sternum center) varied with the posture in a repeatable pattern (Figure 6). While most postural differences were statistically different, their evolutions were small when compared to the large subject-to-subject variations (Figure 6).

All frames and bony parameters are provided in Appendix A.

Table 2: Angle of the S1-T1 axis with the vertical direction (in degrees). Averages and standard deviations are calculated based on n=9 (except for forward-flexed, n=8).

	SUPINE	SEATED	STANDI	FWFLEX
M01	-88	-24	-3	52
M02	-88	-21	-3	n/a
M03	-88	-21	-2	41
M04	-88	-25	-2	48
M05	-88	-20	-2	49
M06	-88	-26	-4	56
F01	-87	-19	-4	58
F02	-89	-20	-3	49
F03	-88	-27	-5	47
Av.	-88	-23	-3	50
S.D.	1	3	1	5

Table 3: Spinal length in mm for all postures and postural variations (for a given subject: maximum difference between any two postures divided by the average of all four postures). Averages and standard deviations are calculated based on n=9 except for forward-flexed (n=8).

	SUPINE	SEATED	STANDI	FWFLEX	Variation
M01	443	448	447	440	1.8%
M02	480	486	487	n/a	1.5%
M03	470	474	469	472	1.1%
M04	449	457	451	450	1.7%
M05	458	465	462	460	1.6%
M06	480	477	466	475	2.8%
F01	485	471	475	484	2.8%
F02	457	470	468	467	2.9%
F03	429	434	433	429	1.3%

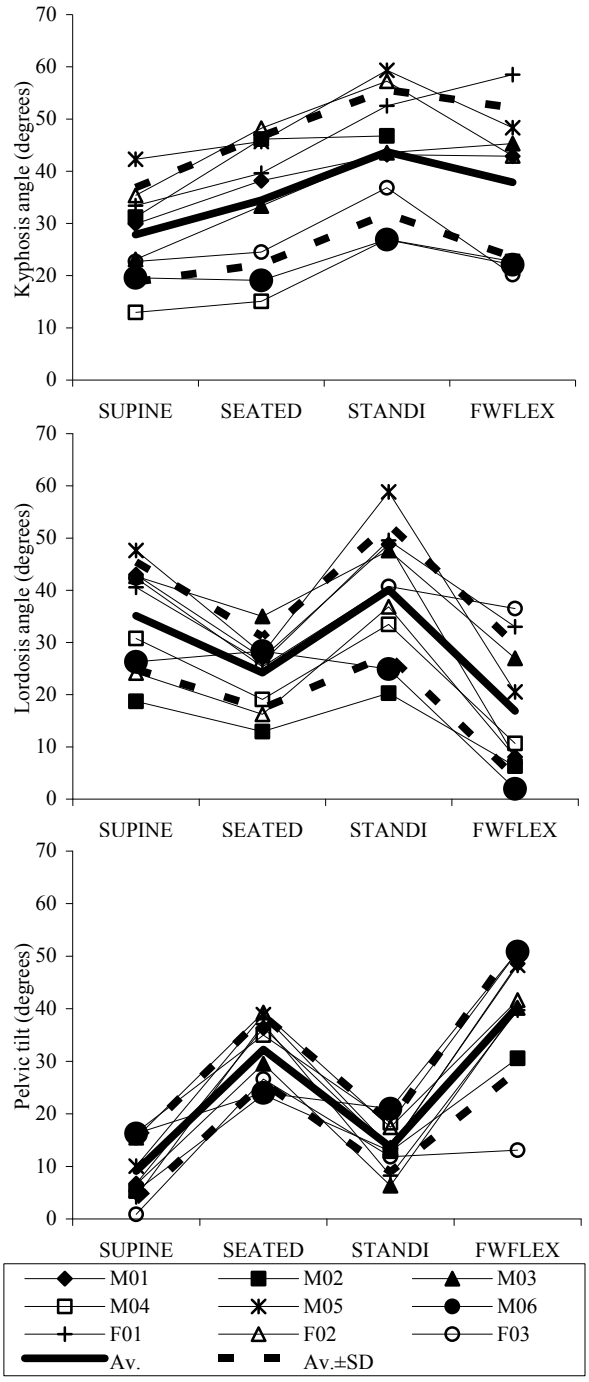

Figure 4: Kyphosis (T4-T12), lordosis (L1-L5) and pelvic tilt angles of all nine subjects. The averages (Av.) and standard deviation (SD) are calculated based on n=9 (except for kyphosis forward-flexed, n=8).

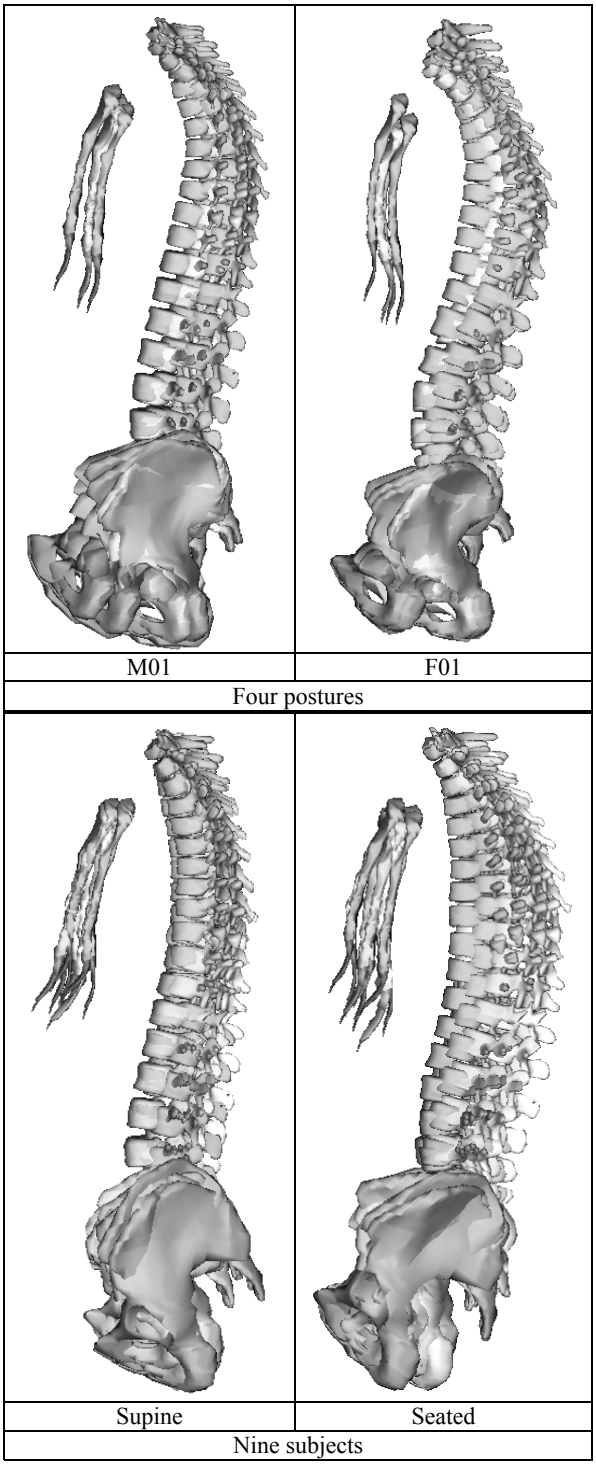

Figure 5: Illustration of the effect of posture vs. subject-to-subject variations on the skeletal system. All models were positioned in the spinal frame (S1-T1). The spinal models of the nine subjects were normalized by the S1-T1 distance.

Table 4: Variation of angle θ1 (pelvic orientation defined by Leung et al., 1979). In degrees.

Subject	SUPINE	SEATED	STANDI	FWFLEX
M01	69	16	18	33
M02	50	14	32	59
M03	56	4	37	40
M04	84	25	5	18
M05	79	17	16	27
M06	62	8	23	48
F01	53	3	36	62
F02	76	18	14	36
F03	61	9	17	66
Av.	66	13	22	43
Std	12	7	11	17

Table 5: Variations of spinal and pelvic parameters between any two postures vs. subject-to-subject variations: average values (Av.) and standard deviations (SD) (n=9, except for kyphosis forward-flexed, n=8). All values are angles in degrees.

a) Variations between any two postures

Source	Supine	Supine	Seated	Supine	Seated	Standi
Target	Seated	Standi	Standi	Fwflex	Fwflex	Fwflex
Kyphosis Av.	7	16	9	10	5	-5
Kyphosis S.D.	5	4	4	9	8	8
Lordosis Av.	-11	5	16	-18	-7	-23
Lordosis S.D.	7	5	10	9	11	12
Pelv. Tilt Av.	23	5	-19	31	8	27
Pelv. Tilt S.D.	8	3	8	9	11	11

b) Subject-to-subject variations

	Supine	Seated	Standi	Fwflex
Kyphosis SD	9	12	12	14
Lordosis SD	10	7	13	13
Pelv. Tilt SD	6	6	5	12

Table 6: Comparison of spinal parameters between this study and literature data. All values are in degrees.

Parameter	Literature		This study
	Reference	Av(SD)	Av (SD)
Kyphosis, standing, T4-T12	Guigui et al. (2003)	40 (9)	44 (12)
	Schwab et al. (2006)	38 (12)	
Lordosis, standing, L1-L5	Mac Thiong et al. (2008)	45 (13)	40 (13)
	Guigui et al. (2003)	43 (11)	
Pelvic Tilt, standing	Guigui et al. (2003)	13 (6)	14 (5)
	Swchab et al. (2006)	13 (7)	
	Boulay et al. (2006)	12 (6)	
Lordosis change Standing/seated	Lord et al. (1997)	15	16
Pelvic angle θ1 Standing	Leung et al. (1979) – 1	26 (8)	22 (11)
	Leung et al. (1979) – 2	21	
Pelvic angle θ1 Seated	Leung et al. (1979) – 2	15	13 (7)

Boulay et al. (2006): n=149; Mac-Thiong et al. (2008): n=120; Schwab et al. (2006): n=25 ; Guigui et al. (2003): n=250 ; Leung et al. (1979): 1: n=28; 2: n=5 ; Lord et al. (1997): n=109. All subjects are healthy adults except Lord et al. (low back pain).

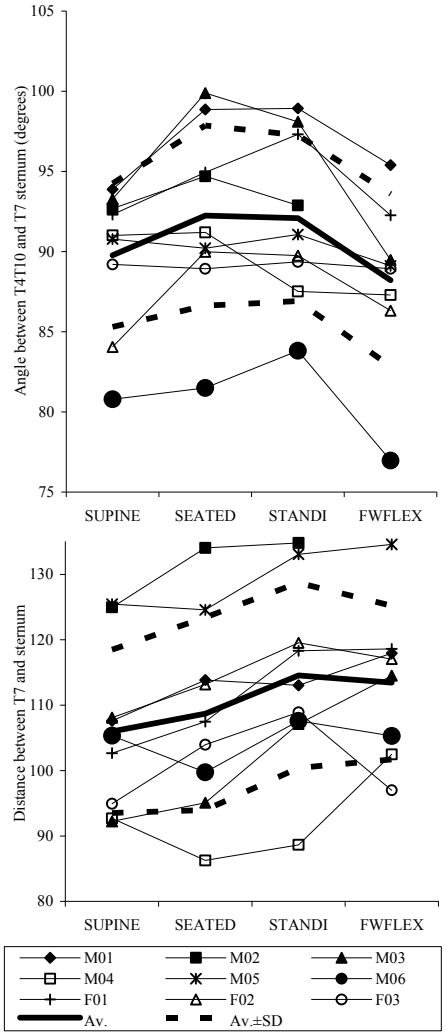

Figure 6: Sternum parameters for all nine subjects. The averages (Av.) and standard deviations (SD) are calculated based on n=9 (except for forward-flexed, n=8).

Effects of posture on soft tissues

Volumes

While the volume of the abdominal object remained almost constant in all positions, the volume of the thoracic cavity was affected by the posture (Figure 7). The abdominal volumes in different postures were not statistically different ($p>0.05$) except the forward-flexed versus seated volumes. However, even in this case, the difference of the averages was less than 3% (difference of 5248 vs. 5410 cm^3). For the thorax, the smallest volume was always in the supine posture and, with the exception of one subject, the largest volume was always in the forward-flexed posture. The thoracic volumes associated with the different postures were all statistically different ($p<0.05$), except the standing and seated volumes which were not statistically different ($p>0.7$). The variations of volume of the thoracic cavity between any two postures were plotted in Figure 8.

Similarly, for the liver, spleen and kidneys, the differences of volumes between postures were not statistically different ($p>0.05$). The only exceptions were the liver volumes between the seated and standing, and seated and forward-flexed postures. However, in these two cases, the differences between the averages were at most 5% (1490 vs. 1568 cm^3). The ratios between standard deviation and average were between 10 and 18% for all objects except for the spleen that had a ratio of 51%. Two subjects with high spleen volumes (308 and 401 cm^3) can partially explain this ratio. If those two subjects were removed, the average and standard deviation would become 145 and 28 cm^3, respectively (ratio of 19%).

There were no obvious correlations between the subject's height, weight, BMI or sex and the volume of the organs. The average volumes of the abdominal object and solid organs are summarized in Table 7. The volumes of solid organs were all similar to volumes published in the literature using MRI, CT or weighting techniques (Table 8).

The detailed volume results are available in Appendix Table B.

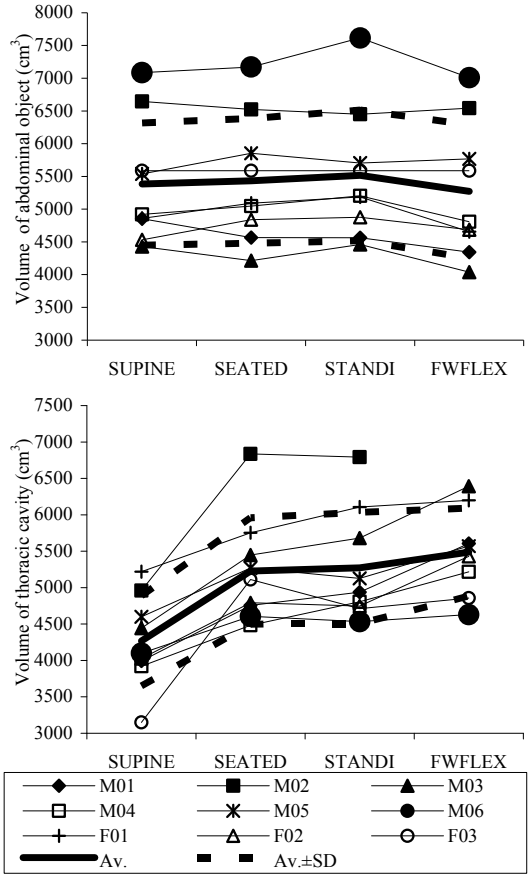

Figure 7: Volumes of the abdominal object and thoracic cavity as a function of posture. The maximum variation of volume across postures for a subject was 11% for the abdomen and 44% for the thorax (calculated as the maximum minus the minimum, divided by the average).

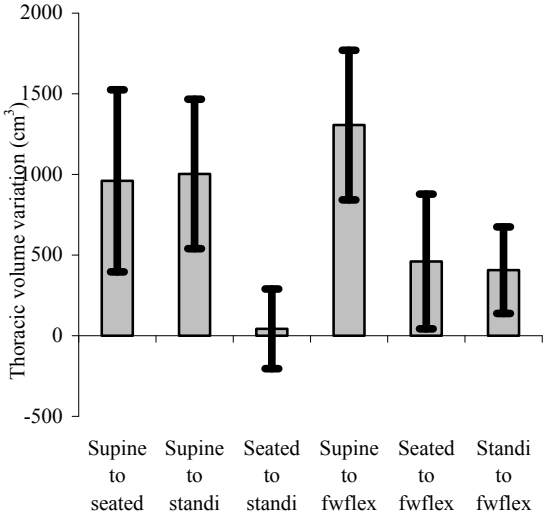

Figure 8: Averages and standard deviations of the variations of volume of the thoracic cavity between any two postures (n=9 except for forward-flexed, n=8).

Table 7: Volumes in cm^3 of the abdominal object and solid organs. Averages (Av.), Standard Deviations (SD), Minimum (Min.) and Maximum (Max.) are calculated based on the average volume in all four postures for nine subjects (n=9).

	Av.	S.D.	Min.	Max.
Abdo. object	5401	967	4286	7220
Liver	1537	160	1302	1791
Spleen	192	98	118	401
Left kidney	150	17	124	180
Right kidney	144	19	122	179

Table 8: Comparison of the volumes of solid organs with literature data for normal adult subjects in supine posture. Average (Av.), Standard Deviation (SD) are in cm^3.

	Literature		This study
	Reference	Av. (SD)	Av. (SD)
Liver	Geraghty et al. (2004) Female n=36	1411 (264)	1537 (160)
	Geraghty et al. (2004) Male n=35	1710 (288)	
	Farraher et al. (2005) n=18	1660 (347)	
	Henderson et al. (1981) n=11	1493	
	Mazonakis et al. (2002) n=27	1480 (230)	
	Grandmaison et al. (2001)* Female n=329	1475 (362)	
	Grandmaison et al. (2001)* Male n=355	1677 (371)	
Spleen	Geraghty et al. (2004) Female n=34	180 (66)	192 (98)
	Geraghty et al. (2004) Male n=47	238 (70)	
	Farraher et al. (2005) n=27	320 (213)	
	Henderson et al. (1981) n=11	219	
	Grandmaison et al. (2001)* Female n=329	140 (78)	
	Grandmaison et al. (2001)* Male n=355	156 (87)	
Left kidney	Geraghty et al. (2004) Female n=31	160 (33)	150 (17)
	Geraghty et al. (2004) Male n=35	201 (29)	
	Cheong et al. (2007) Male n=61	205 (35)	
	Cheong et al. (2007) Female n=89	156 (34)	
	Grandmaison et al. (2001)* Female n=329	136 (37)	
	Grandmaison et al. (2001)* Male n=355	160 (41)	
Right kidney	Geraghty et al. (2004) Female n=38	153 (33)	144 (19)
	Geraghty et al. (2004) Male n=45	185 (32)	
	Cheong et al. (2007) Male n=61	202 (36)	
	Cheong et al. (2007) Female n=89	154 (33)	
	Grandmaison et al. (2001)* Female n=329	135 (39)	
	Grandmaison et al. (2001)* Male n=355	162 (39)	

All data obtained on live subjects except Grandmaison et al. (2001)

* Assuming a specific density of 1 g/cm^3 for all solid organs.

Organ Position

When the posture changed, the solid organs essentially moved in a sagittal plane (as illustrated by the small variations of along the Y-axis in the Figure 9). The main motion was along the Z-axis (S1-T1 axis), with variations of positions up to approximately 35 to 40 mm between the supine and the other postures. This motion was not associated with the displacement of the closest lumbar vertebra (L1, L2 or L3). Along the X-axis (antero-posterior), the solid organs did not appear to follow the closest vertebra. A graphical illustration of these variations on two subjects is provided in Figure 10.

The thoracic cavity and the abdominal object followed similar trends: the motion of their center was mainly in a sagittal plane and along the Z-axis. The corresponding curves are provided in Figure 11 for reference.

For the solid organs positions along the Z-axis, the supine posture was statistically different from all the other postures ($p<0.004$). The other postures were not statistically different from one another ($p>0.05$) except for the spleen position in seated vs. standing posture (9 mm difference in average). Along the X-axis, most postural differences were not statistically significant ($p>0.05$) except the right kidney in supine vs. standing posture ($p=0.039$, difference of position of 15 mm). The distance between L4 and the skin was statistically different between any two postures. The most notable change was between the supine and the other postures. It reached up to 68 mm between the supine and forward-flexed posture. Key differences in position for any two postures are summarized in Table 9. The displacements of the liver, spleen and diaphragm along the Z-axis were not statistically different from one another for the same change of posture.

Besides the postural variations, the anatomical position of the kidneys with respect to the other organs and the diaphragm varied greatly from subject-to-subject as illustrated on Figure 12.

The centers of all soft objects in all postures are provided in Appendix Table C.

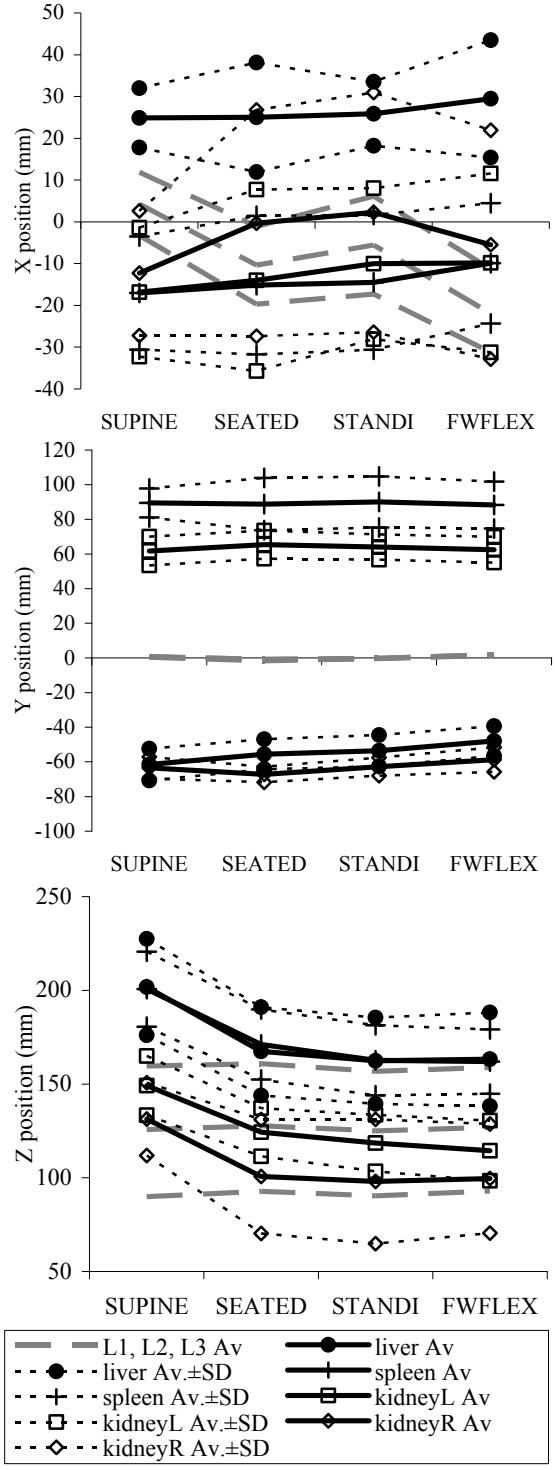

Figure 9: Effect of the posture on the coordinates of the center of solid organs in the spinal frame. Averages (Av.) and standard deviations (SD) are based on nine subjects. For clarity, the standard deviations for the vertebrae (L1, L2, L3) are not shown.

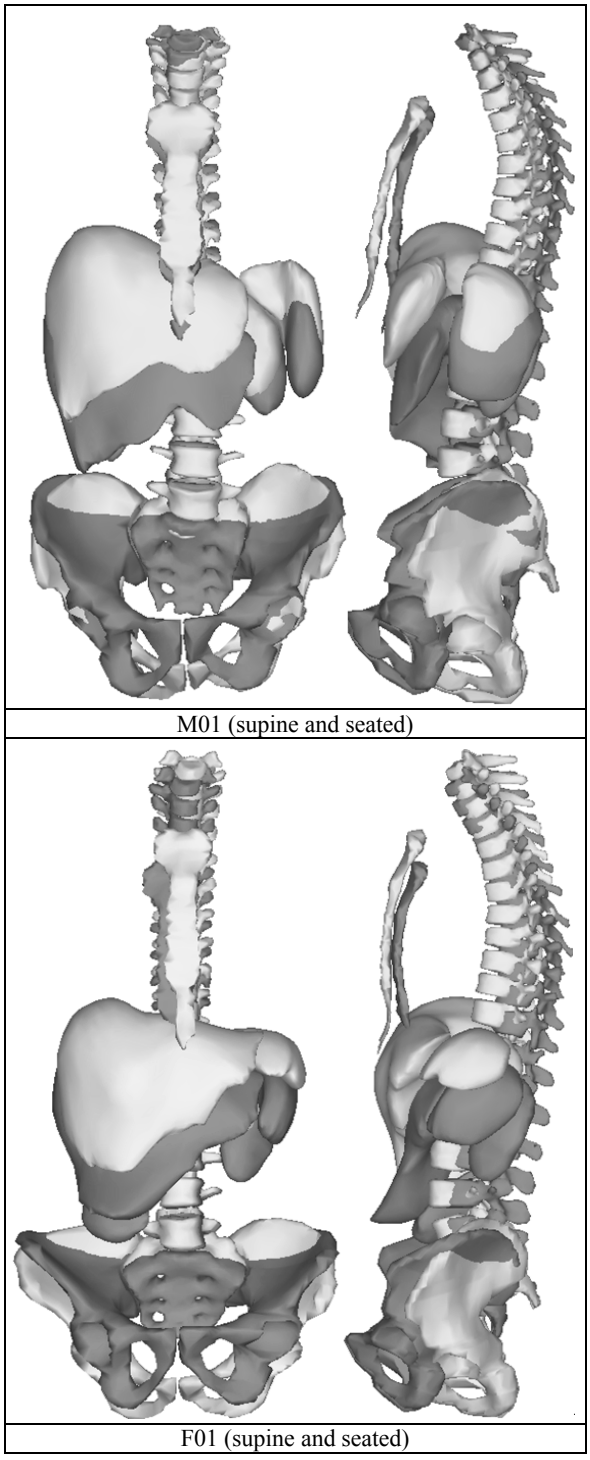

Figure 10: Illustration of the upward motion of the solid organs between the supine and the seated posture. Only the skeletal components, liver, spleen and kidneys are shown. For the comparisons, the spinal frames of the models are aligned.

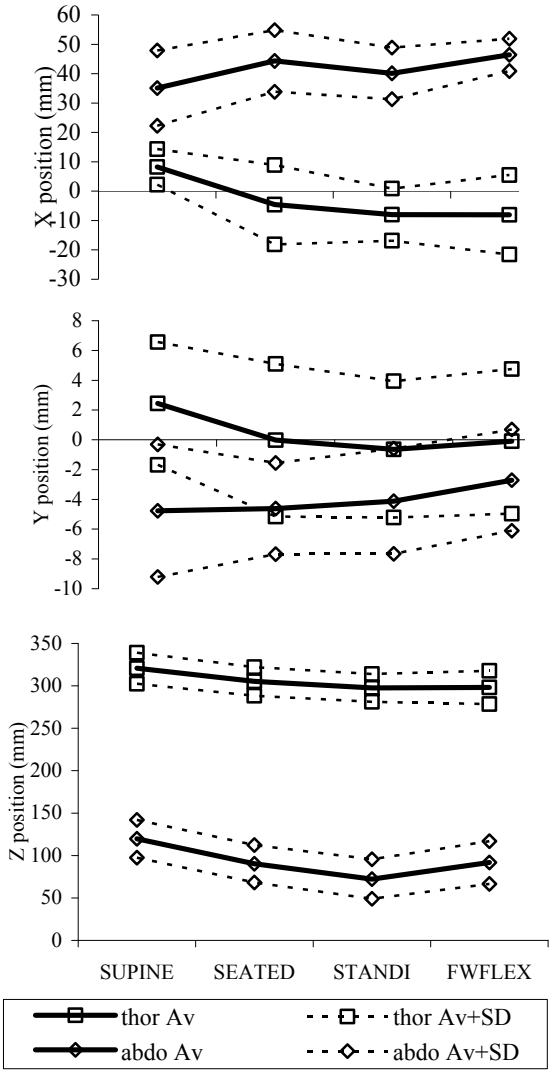

Figure 11: Effect of the posture on the coordinates of the center of the thorax and abdomen objects in the spinal frame. Averages (Av.) and standard deviations (SD) are based on n=9 (except for the thorax cavity forward-flexed n=8).

Table 9: Difference of position (mm) of solid organs (center) between any two postures along the Z-axis of the spinal frame (S1-T1). Average (Av.) and Standard Deviation (SD) are based on nine subjects.

Source	Supine	Supine	Seated	Supine	Seated	Standi
Target	Seated	Standi	Standi	Fwflex	Fwflex	Fwflex
Z liver Av.	-34	-39	-5	-39	-4	1
Z liver SD	16	14	9	15	9	8
Z spleen Av.	-30	-38	-8	-39	-9	-1
Z spleen SD.	13	11	8	7	11	8
Z kidneyL Av.	-25	-31	-6	-35	-10	-4
Z kidneyL SD	8	11	12	11	13	8
Z kidneyR Av.	-31	-33	-3	-32	-1	2
Z kidneyR SD	16	18	14	11	13	14
MaxZ S1-Diaph Av	-36	-41	-5	-39	-3	2
MaxZ S1-Diaph SD	15	15	9	15	8	9
X dist. L4-Skin Av.	52	34	-18	68	16	34
X dist. L4-Skin Av.	11	9	11	13	13	10

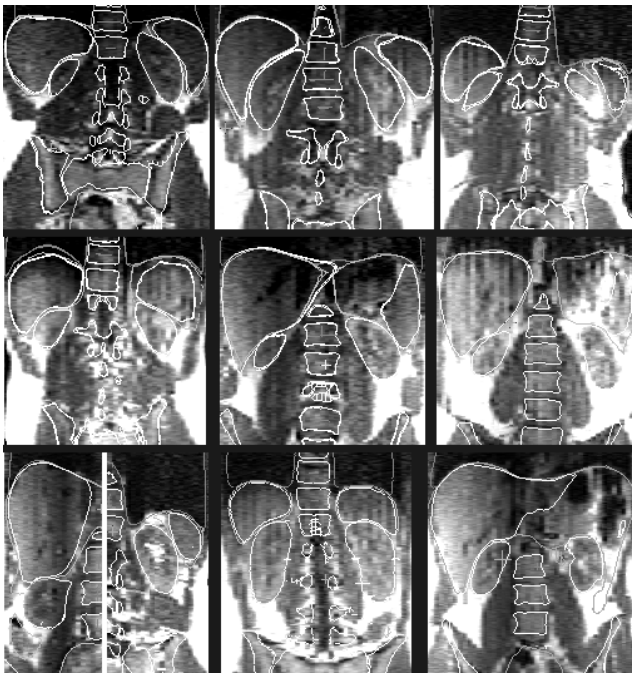

Figure 12: Variations of the positions of the kidneys among the nine subjects (M01 to M06 and F01 to F03 from top left to bottom right). The images are coronal sections reconstructed from sagittal slices in the seated posture. Two images were used for F01 as both kidneys were not in the same coronal plane. The lines represent the intersection between the MRI slice and the objects. Depending on the subject, the right kidney (left of the picture) is in contact with the diaphragm (M01 to M03, F03) or away from the surface (e.g. below the spleen). Similarly, the position of the left kidney varies greatly with respect to the liver and the diaphragm (e.g. M02 vs. F01).

Organ Shapes (vs. position vs. size)
After alignment using the ICP method, the thoracic cavity meshes associated with the four postures were very close in regions away from the diaphragm as illustrated in Figure 13a. For example, the average mesh-to-mesh distance over the complete thoracic mesh between the standing and seated posture was 3 mm. However, the supine thorax cavity greatly differed from the other postures in the region of the diaphragm. When limiting the meshes to the region of the diaphragm (Figure 13b), the maximal mesh-to-mesh distance between supine and standing was 63 mm, with an average distance of 39 mm. This difference was of the same order as the subject-to-subject variability (Figure 13c).

When comparing the shapes of the abdominal object (Figure 14, top), the supine model differed from the other postures by its depth in the lumbar region and by its height in the diaphragmatic region. However, there were similarities with the Figure 5 in the pelvic region as the abdominal object followed the pelvis. This difference between the supine and other postures was of the same order as the subject-to-subject variability (Figure 14 bottom).

When comparing the shapes of the liver for different postures, small changes were visible in particular near the diaphragm (Figure 15a). Those changes were relatively limited and of similar amplitude as the subject-to-subject variations (Figure 15b). For the spleen, the shape of the organ was very different from subject to subject (Figure 16a), and in comparison, the postural effects were very small (Figure 16b). Finally, the shapes of the kidneys were very similar among subjects and the organs shapes were essentially unaffected by the postural changes (Figure 17).

The diagonal values of the inertial matrices of the solid organs (expressed in the spinal frame moved to the center of the object) were compared between any two postures. Out of 72 combinations (six postural pairs times four organs times three inertial values), only 12 differences were statistically significant. These combinations were associated with differences of less than 8% of the average (liver, 4 comparisons), and less than 25% in the 8 others (kidneys and spleen). The maximum difference was for the right kidney between the supine and forward-flexed inertial values about the X-axis ($1.15x10^8$ vs. $0.92x10^8$ mm^4). The inertial matrices of all objects are provided in Appendix Table D and Appendix Table E.

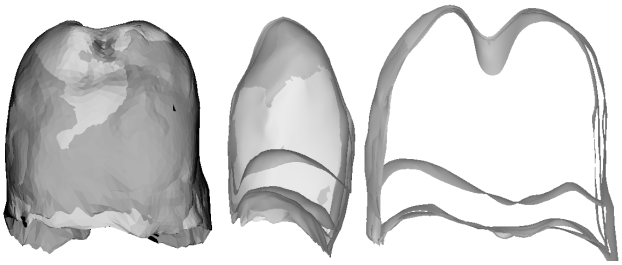

a) Thoracic cavity of M01 in four postures after ICP alignment. Left: the different objects are well superimposed and are difficult to distinguish from one another. Center: same models partially shown from a lateral point of view. Right: sections in a coronal plane. The supine section is different from the other ones in the region of the diaphragm.

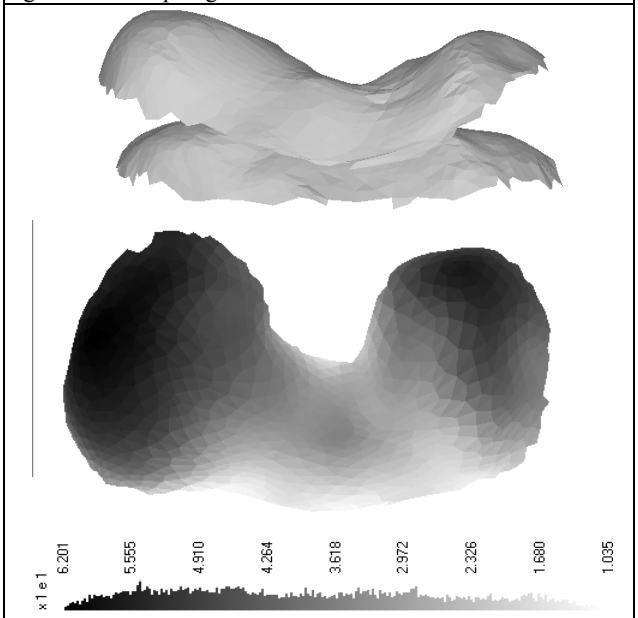

b) Mesh-to-mesh bilateral distance map from diaphragm to diaphragm between M01 supine and M01 standing. The scale of the map is in millimeters.

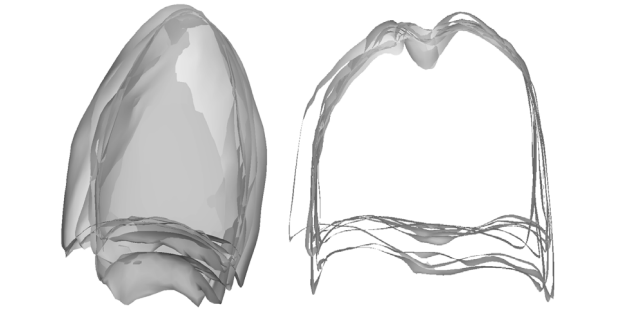

c) Thoracic cavity for all subjects in the seated postion after ICP alignment. The models are unscaled. Left: models partially shown from a lateral point of view. Right: section in a coronal plane.

Figure 13: Comparison of the effects of posture and subject-to-subject variability on the shape and size of the thoracic cavity.

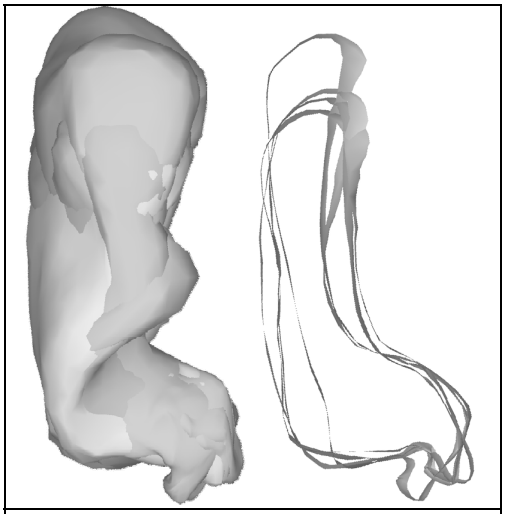

M01 (four postures)

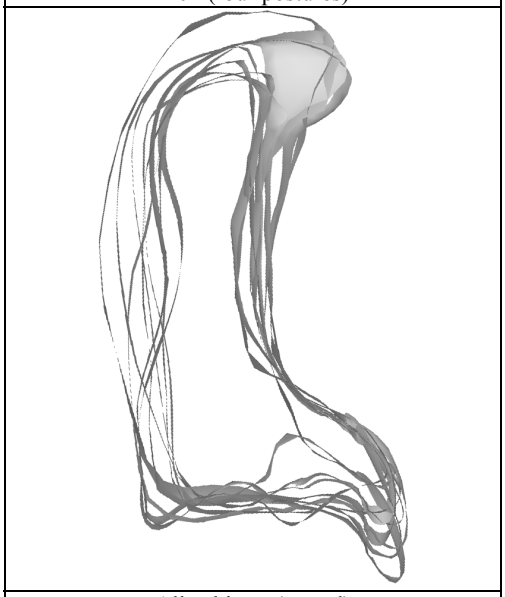

All subjects (seated)

Figure 14: Comparison of the effects of posture and subject-to-subject variability on the shape and size of the abdominal object (sagittal view, after ICP alignment). Top: M01 models from a lateral point of view and mid-sagittal section. The supine model differs from the others by a higher diaphragmatic surface and a thinner profile. Bottom: Mid-sagittal section of seated models for all subjects. All models are unscaled.

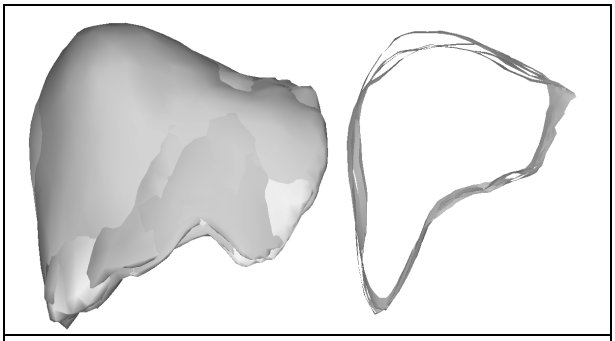

a) M01 (four postures). Left: superimposed models. Right: coronal section. The supine model differs from the others, in particular by a higher diaphragmatic surface (in the order of 10 mm). It is almost coincident in other regions

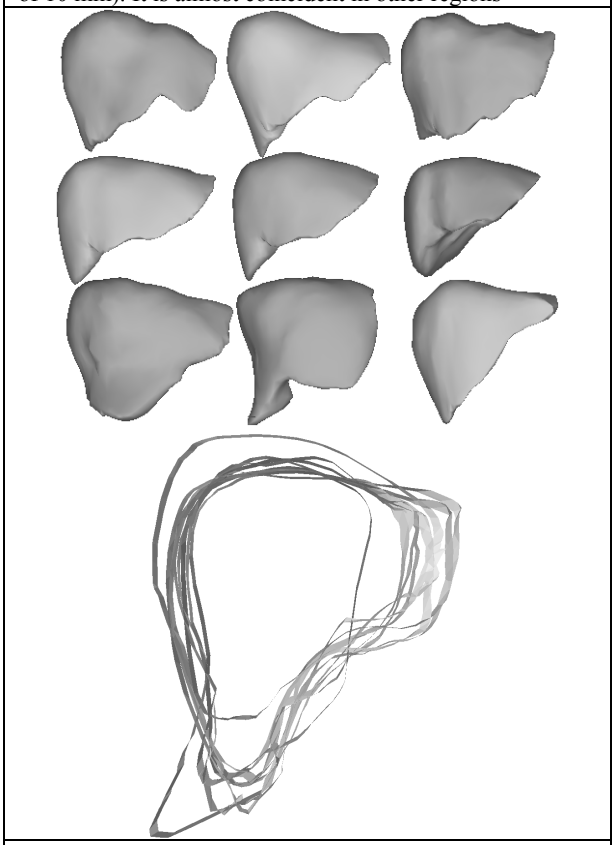

b) All subjects (seated). Top: from M01 to F03 from top left to right bottom. Bottom: coronal section of the nine models.

Figure 15: Comparison of the effects of posture and subject-to-subject variability on the shape and size of the liver object. All models are unscaled and seen from an anterior point of view. ICP alignment was performed for the superimposed models.

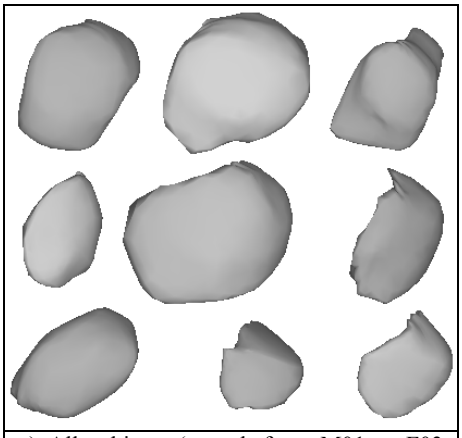

a) All subjects (seated, from M01 to F03 from top left to right bottom)

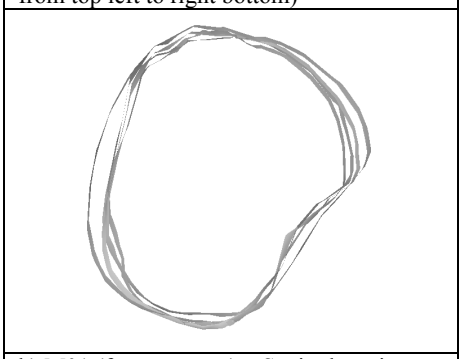

b) M01 (four postures) – Sagittal section

Figure 16: Comparison of the effects of posture and subject-to-subject variability on the shape and size of the spleen. All models are unscaled and seen from a lateral point of view. ICP alignment was performed for the superimposed models.

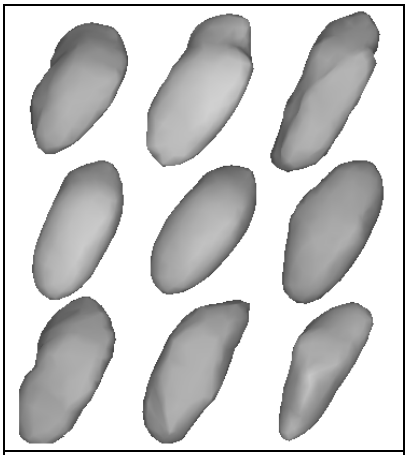

a) All subjects (seated, from M01 to F03 from top left to right bottom)

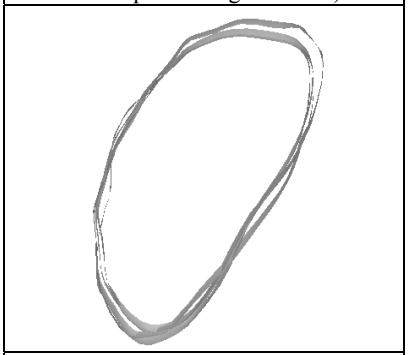

b) M01 (four postures) – Sagittal section

Figure 17: Comparison of the effects of posture and subject-to-subject variability on the shape and size of the left kidney. All models are unscaled and seen from a lateral point of view. ICP was performed for the superimposed models.

DISCUSSION

Nine subjects were imaged in four postures using a Fonar Upright MRI. Polygonal models of key anatomical structures of the abdomen and the thorax were registered from the images using a custom toolbox. The qualitative and quantitative analysis of the images and models allowed illustration and quantification of the respective effects of posture and subject-to-subject variability on the position and shape of the abdominal and thoracic organs.

All skeletal parameters were affected by the posture. The forward-flexed posture was generally associated with larger subject-to-subject variations (e.g. variations of spine position in the global frame). One explanation could be that it was the posture with the least constraint on the subject. It was the only posture where the back was not against a flat surface, leaving the subjects free to choose different combinations of pelvic tilt, lordosis and kyphosis to reach the approximate 45 degrees back angle. For the other postures, the contact with a flat surface at the pelvis and around the T9 level most likely limited the possible spine angles.

In terms of limitations, the portion of the imaging coil located between the back of the subject and the flat surface may have affected the overall back angle since the coil only covers the imaged region and does not span from pelvis to T9. The coil thickness was approximately 2 to 3 cm, which is small compared to the distance between the contact areas (pelvis to T9). Cushions were also used to compensate for this thickness away from the coil.

The thoracic cavity was the only object whose volume was greatly affected by the posture (1000 cm^3

or more). The variations of volume between any two postures were not statistically different for the abdominal object and solid organs with the exception of the liver for two of the postural changes. However, even in this case, the differences were small (less than 5% of the average). It is unknown if these differences are an artifact due to measurement errors or if physiological changes could be involved, as the blood flow in the liver can be posture dependant (Brown et al., 1989). In general, the overall conservation of volume suggests that changes due to digestion, urination or other biological processes that could have occurred during the four-hour scanning session did not greatly affect the volume estimations.

The pelvic tilt was the parameter that changed with the most repeatable pattern for all the subjects, even for the forward-flexed position, suggesting that it was key in determining the position of the skeleton. When analyzing the overall organ motion associated with the posture, two important constraints seem to be that the volume of the abdominal contents remains constant and the shape of the rib cage does not change. Therefore:

- When going from seated to supine, the depth of the abdomen decreases as illustrated by the reduction of the L4-to-skin distance. This reduction, combined with the conservation of the volume of the abdominal object, is associated with increased dimensions in the other directions. The increased height in the direction of the thorax results in a motion of the diaphragm and a reduction of the volume of the thoracic cavity.
- The effect of gravity on the abdominal contents is less important between all road user postures, even though it can be detected on the depth of the abdomen in the forward-flexed position.
- In all cases, the overall abdominal contents deform to follow the spinal curvature and pelvic tilt. This deformation is the most important factor when going between road user postures.

In terms of amplitude, the average motion of the abdominal organs reached 39 mm for the liver between the supine and standing postures. This is similar to the results published by Wade (1954) on the motion of the right leaf of the diaphragm between the standing and supine position (overage of 38 mm when subtracting the average distance between the right leaf and the iliac crest in the supine and standing positions). The amplitude of motion was also similar for the spleen and the kidneys (Table 9), despite the fact the kidneys are retroperitoneal.

Furthermore, the difference of solid organ shapes between the supine and the other postures were small (Figure 15 to Figure 17), suggesting that their motion was mostly rigid during the postural changes. The change of the abdominal object shape was therefore essentially due to deformations of the hollow organs and surrounding tissues, mainly in the regions above the pelvis (illustrated by Figure 14 and the L4-to-skin distance). Based on the comparison of the inertial matrices, the mass distribution (assuming a constant density) along the axes of the spinal frame was unaffected by the posture in most cases. However, even for the most significant change (25%), the interpretation was difficult as it was not possible to distinguish between the object deformation and its rigid rotation solely based on inertial data. Moreover, for the current application, the relevance of principal axes is unclear as they can be very sensitive to small changes of shape for rounded objects. Future work will be conducted to determine organ shape transformation functions between any two postures.

One important limitation of the study was the lack of estimation of the error associated with the complete measurement process. A basic evaluation of the toolbox had suggested that, for a voxel size larger than the one used in the current study, registration errors could be lower than 11.2% of the volume or 4.4 mm for 95% of the samples of a surface. The effects of other possible sources of errors including the rigid image registration, motion artifacts (due to subject motion, breathing, heartbeat), or the operator dependence during the registration process were not evaluated. However, when comparisons were possible, skeletal parameters, organ volumes or organ motion parameters from the current study were in good agreement with existing literature data, for both averages and standard deviations (Table 6 and Table 8), thus suggesting that the overall process could be appropriate for the current objectives.

Another limitation of the study was the subject population. All subjects were within the same age range and had normal Body Mass Indexes. This may explain the lack of relation between BMI, weight and other factors (e.g. abdominal volume). However, one could assume that the location and volume of the abdominal contents would be different for overweight or obese subjects. In addition, there was no clear relation between stature and organ size. One reason may be that there was only one large male (1.91 m) and one medium female (1.62 m) included in the subject population and that all other subjects had heights between 1.69 m and 1.83 m. The results of the current study are specific to the subject population (young adults with normal BMI). They may not apply

to elderly individuals or individuals with high BMI since muscle tone and fat contents may affect the position or the motion of the organs. More work would be needed to characterize such populations.

Consequences for FE modeling and injury prediction

The data generated in this study can be used for the positioning of finite element models in road user positions. For the seated (driving) vs. standing (pedestrian) posture, the study suggests that the changes of soft organ shape and position could be very limited and that the main parameters to consider could be the change of pelvic angle and spinal curvature. However, the study was conducted using a rigid seat and it is likely that the use of a deformable seat would affect the spinal geometry. For the forward-flexed posture, the postural effects on the abdominal soft tissues are more important yet the variety of possible riding positions could affect the results also.

The study suggests that the use of traditional supine MRI as a geometrical base for road user models may be problematic even after correction of the changes of spinal curvature because it would underestimate the depth of the abdomen and induce an error on the position of the solid organs. This error of up to 40 mm on the center of the liver would be critical if the model aims to predict injury based on stress or strain because there would be a mismatch between the strain calculated and the location of the organ.

Furthermore, the high subject-to-subject variability found in the current study, both in terms of organ size and organ anatomical location, could also be problematic for strain-based injury prediction using an "average model". For example, it is unclear if an average size spleen (192 cm^3) can represent a spleen population that varied from 120 to 400 cm^3, especially if there was a relation between the organ size and the injury risk. Another example is the variation of anatomical location of the kidney with respect to the diaphragm, which may also have an influence on the injury risk. Possible effects of such variations should be investigated in the future.

From the mechanical standpoint, it must be noted that the change of position of the abdominal organs between the supine and the other postures occurred under a very small load. If an average density of 1 kg per liter were used, the mass of the abdominal object would be approximately 5.4 kg. The change of organ position would be associated with the change of direction of a force of 54 N from the proximal-distal to the antero-posterior direction, plus some additional weight from the anterior surrounding muscles. It is unknown if such a deformation mode is likely in the automotive setting where loads are much higher but are applied differently (very fast belt loading for example). However the current data suggests that there would be vey little resistance to oppose such a motion (besides the inertia) if it were to occur.

SUMMARY AND CONCLUSIONS

Positional MRI scanning was performed on the thorax and the abdomen of nine subjects in four postures: supine, seated, standing and forward-flexed. The data were processed using a custom registration toolbox and thirty-six models of the subjects were generated using this technique. The qualitative and quantitative analysis of the images and models allowed to characterize the respective effects of posture and subject-to-subject variations on the position and shape of the abdominal organs.

The supine posture was associated with a motion of the solid organs of up to 40 mm when compared with the other postures. The differences between the standing, seated and forward-flexed postures were very limited in comparison, making the variations of skeletal parameters (pelvis and spine) the most important when comparing these three postures. This suggests that abdominal geometry should be corrected for organ motion if supine datasets are used as a basis for finite element modeling of the abdomen. Some of the subject-to-subject variations of organ size and organ position were large (spleen and kidney), suggesting that the subject-to-subject variability could also be important for finite element modeling.

This study also provides values for key parameters that can be used to facilitate the development and positioning of different road user models (occupant, pedestrian and cyclist). The method that was developed is non-invasive and can be used to study the effects of other postures (using deformable seats or other bicycle positions) or subject-to-subject variations using a more diverse population.

ACKNOWLEDGMENTS

This study was made possible by a Marie Curie grant (MIRG-CT-2006-036595) from the European Commission. The authors would like to acknowledge Bev McLennan (University of Aberdeen), Jean-Pierre Verriest, Richard Roussillon, Yves Caire, Julia Samorezov and Julien Causse (INRETS) for their precious help on the project.

REFERENCES

Aspert, N., Santa-Cruz, D., and Ebrahimi, T. (2002). MESH: measuring errors between surfaces using the Hausdorff distance. In Multimedia and Expo, (2002). ICME '02. Proceedings. 2002 IEEE International Conference on, pp. 705-708 vol.1.

Bertrand, S., Skalli, W., Delacherie, L., Bonneau, D., Kalifa, G., and Mitton, D. (2006). External and internal geometry of European adults. Ergonomics 49, 1547-1564.

Blackall, J. M., Ahmad, S., Miquel, M. E., McClelland, J. R., Landau, D. B., and Hawkes, D. J. (2006). MRI-based measurements of respiratory motion variability and assessment of imaging strategies for radiotherapy planning. Phys Med Biol 51, 4147-4169.

Boulay, C., Tardieu, C., Hecquet, J., Benaim, C., Mouilleseaux, B., Marty, C., et al. (2006). Sagittal alignment of spine and pelvis regulated by pelvic incidence: standard values and prediction of lordosis. European Spine Journal: Official Publication of the European Spine Society, the European Spinal Deformity Society, and the European Section of the Cervical Spine Research Society, 15(4), 415-422. doi: 10.1007/s00586-005-0984-5.

Brown, H. S., Halliwell, M., Qamar, M., Read, A. E., Evans, J. M., & Wells, P. N. (1989). Measurement of normal portal venous blood flow by Doppler ultrasound. Gut, 30(4), 503-509.

Brandner, E. D., Wu, A., Chen, H., Heron, D., Kalnicki, S., Komanduri, K., Gerszten, K., Burton, S., Ahmed, I., and Shou, Z. (2006). Abdominal organ motion measured using 4D CT. Int. J. Radiat. Oncol. Biol. Phys 65, 554-560.

Cheong, B., Muthupillai, R., Rubin, M. F., & Flamm, S. D. (2007). Normal values for renal length and volume as measured by magnetic resonance imaging. Clinical Journal of the American Society of Nephrology: CJASN, 2(1), 38-45.

Farraher, S. W., Jara, H., Chang, K. J., Hou, A., & Soto, J. A. (2005). Liver and spleen volumetry with quantitative MR imaging and dual-space clustering segmentation. Radiology, 237(1), 322-328.

Frøkjaer, J. B., Liao, D., Steffensen, E., Dimcevski, G., Bergmann, A., Drewes, A. M., and Gregersen, H. (2007). Geometric and mechanosensory properties of the sigmoid colon evaluated with magnetic resonance imaging. Neurogastroenterol Motil 19, 253-62.

Gangnet, N., Dumas, R., Pomero, V., Mitulescu, A., Skalli, W., Vital, J.M.,(2006). Three-Dimensional Spinal and Pelvic Alignment in an Asymptomatic Population. Spine 31(15), E507-512.

Gemery, J. M., Nangia, A. K., Mamourian, A. C., and Reid, S. K. (2007). Digital three-dimensional modelling of the male pelvis and bicycle seats: impact of rider position and seat design on potential penile hypoxia and erectile dysfunction. BJU Int 99, 135-140.

Geraghty, E. M., Boone, J. M., McGahan, J. P., & Jain, K. (2004). Normal organ volume assessment from abdominal CT. Abdominal Imaging, 29(4), 482–490.

Guigui, P., Levassor, N., Rillardon, L., Wodecki, P., & Cardinne, L. (2003). [Physiological value of pelvic and spinal parameters of sagital balance: analysis of 250 healthy volunteers]. Revue De Chirurgie Orthopédique Et Réparatrice De L'appareil Moteur, 89(6), 496-506.

de la Grandmaison, G. L., Clairand, I., & Durigon, M. (2001). Organ weight in 684 adult autopsies: new tables for a Caucasoid population. Forensic Science International, 119(2), 149-154.

Henderson, J. M., Heymsfield, S. B., Horowitz, J., & Kutner, M. H. (1981). Measurement of liver and spleen volume by computed tomography. Assessment of reproducibility and changes found following a selective distal splenorenal shunt. Radiology, 141(2), 525-527.

Langen, K. M., and Jones, D. T. (2001). Organ motion and its management. Int. J. Radiat. Oncol. Biol. Phys 50, 265-278.

Lord, M. J., Small, J. M., Dinsay, J. M., & Watkins, R. G. (1997). Lumbar lordosis. Effects of sitting and standing. Spine, 22(21), 2571-2574.

Lotz, H. T., van Herk, M., Betgen, A., Pos, F., Lebesque, J. V., and Remeijer, P. (2005). Reproducibility of the bladder shape and bladder

shape changes during filling. Med Phys 32, 2590-2597.

Leung, Y. C., Tarrière, C., Lestrelin, D., Got, C., Guillon, F., Patel A. and Hureau, J. (1982) Submarining Injuries of 3 Pt. Belted Occupants in Frontal Collisions – Decription, Mechanisms and Protection. Proceedings of the 26th Stapp Car Crash Conference. Ann Arbor, Michigan, USA

Mazonakis, M., Damilakis, J., Maris, T., Prassopoulos, P., & Gourtsoyiannis, N. (2002). Comparison of two volumetric techniques for estimating liver volume using magnetic resonance imaging. Journal of Magnetic Resonance Imaging: JMRI, 15(5), 557-563. doi: 10.1002/jmri.10109.

Mirtich, B. (1996). Fast and accurate computation of polyhedral mass properties. J. Graph. Tools 1, 31-50. Also available online (accessed August 4, 2009): http://www.cs.berkeley.edu/~jfc/mirtich/massProps.html

Mac-Thiong, J., Wang, Z., de Guise, J. A., & Labelle, H. (2008). Postural model of sagittal spino-pelvic alignment and its relevance for lumbosacral developmental spondylolisthesis. Spine, 33(21), 2316-2325.

Rohlfing, T., Maurer, C. R., O'Dell, W. G., and Zhong, J. (2004). Modeling liver motion and deformation during the respiratory cycle using intensity-based nonrigid registration of gated MR images. Med Phys 31, 427-432.

Schwab, F., Lafage, V., Boyce, R., Skalli, W., & Farcy, J. (2006). Gravity line analysis in adult volunteers: age-related correlation with spinal parameters, pelvic parameters, and foot position. Spine, 31(25), E959-967.

Stokes, I. A. (1994). Three-dimensional terminology of spinal deformity. A report presented to the Scoliosis Research Society by the Scoliosis Research Society Working Group on 3-D terminology of spinal deformity. Spine 19, 236-248.

Trochu, F. (1993). A contouring program based on dual kriging interpolation. Engineering with Computers, 9(3), 160–177.

Vrtovec, T., Pernus, F., & Likar, B. (2009). A review of methods for quantitative evaluation of spinal curvature. European Spine Journal: Official Publication of the European Spine Society, the European Spinal Deformity Society, and the European Section of the Cervical Spine Research Society, 18(5), 593-607. doi: 10.1007/s00586-009-0913-0.

Wade, O. L. (1954). Movements of the thoracic cage and diaphragm in respiration. J. Physiol. (Lond.) 124, 193-212.

APPENDIX

Appendix A: Bony parameters

Spinal and pelvic parameters were computed using definitions from the clinical literature (Stokes 1994), meaning that the parameters were computed from two-dimensional projections (similar to methods used for biplanar Xrays, Gangnet et al., 2006). A method that is described by Vrtovec et al. (2009) was used to calculate the spinal parameters. First, the spinal curvature was modeled with a spline curve passing through three landmarks of the vertebral bodies: the center of the body and the centers of the inferior and superior plates. Then the angles of kyphosis and lordosis were computed from the first derivative (i.e., tangents to the curve) projected in sagittal plane. Based on Vrtovec et al. (2009), this method offers “an improved intra-observer variability as well as a high inter-observer reliability”. The parameters are illustrated in Figure A-1.

For the pelvis, two parameters were selected to quantify the pelvic rotation:

- the pelvic tilt angle, that is often used to predict lordosis angle, and
- the θ1 angle defined in Leung et al. (1979).

The pelvic tilt angle is the 2D sagittal angle “defined by the line through midpoint of the sacral plate and midpoint of the femoral heads axis” and the Z-axis (Boulay et al., 2006). The “pelvic tilting is positive when the sacral plate is behind the hip and negative when it is in front of it” (Boulay et al., 2006).

The angle θ1 is the angle between the X-axis in the global frame and the line passing through the center of the upper face of the sacrum and the anterior superior iliac spine (Leung et al., 1979).

An illustration of both pelvic parameters is provided in Figures A-2 and A3.

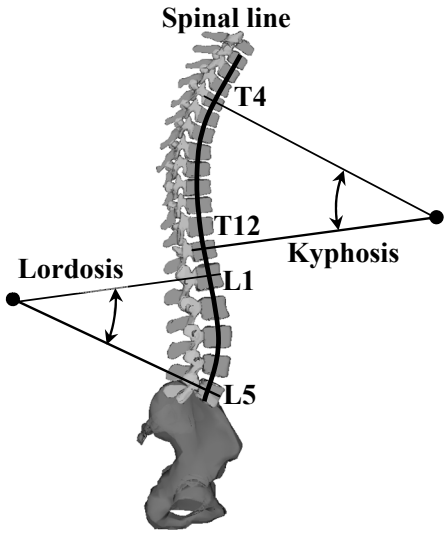

Figure A-1: Computation of the clinical spinal parameters (T4-T12 kyphosis and L1-L5 lordosis).

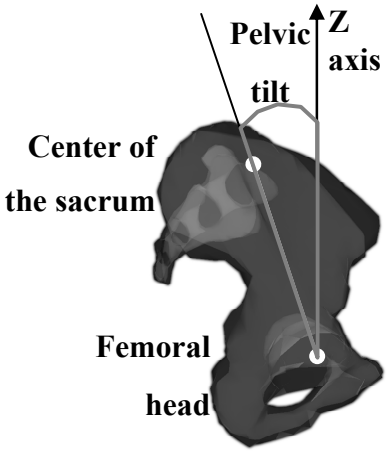

Figure A-2: Computation of the pelvic tilt (Boulay et al. 2006)

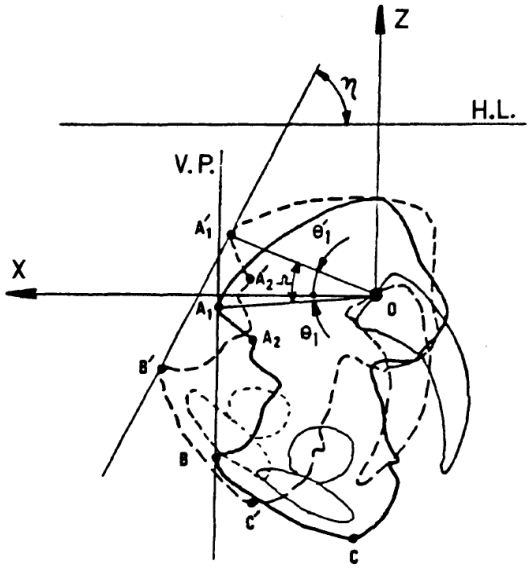

Figure A-3: Angle θ1. Illustration from Leung et al. (1979).

Appendix Table A: Position of the spinal frame in the global frame and skeletal parameters.

		Rot. X global (degrees)	Rot. Y global (degrees)	Rot. Z global (degrees)	Spinal length (mm)	Kyphosis (degrees)	Lordosis (degrees)	Pelvic tilt (degrees)	angle T4-T10 T7sternum (degrees)	Dist. T7 sternum (mm)
SUPINE	M01	-167	-88	-170	443	30	43	7	94	108
	M02	-8	-88	-8	480	31	19	5	93	125
	M03	-74	-88	-70	470	23	43	7	93	92
	M04	15	-88	17	449	13	31	16	91	93
	M05	-34	-88	-32	458	42	48	10	91	125
	M06	-32	-88	-28	480	20	26	16	81	105
	F01	-154	-87	-153	485	33	41	4	92	103
	F02	-64	-89	-61	457	35	24	15	84	108
	F03	-174	-88	-172	429	23	42	1	89	95
	AV.	-77	-88	-75	461	28	35	9	90	106
	SD.	71	1	72	19	9	10	6	4	12
SEATED	M01	0	-24	-2	448	38	27	36	99	114
	M02	0	-21	0	486	46	13	24	95	134
	M03	-1	-21	4	474	33	35	30	100	95
	M04	0	-25	2	457	15	19	35	91	86
	M05	-1	-20	-1	465	46	28	39	90	125
	M06	-1	-26	2	477	19	28	24	81	100
	F01	-1	-19	4	471	40	26	37	95	107
	F02	0	-20	-1	470	48	16	39	90	113
	F03	0	-27	-1	434	25	25	27	89	104
	AV.	-1	-22	1	465	34	24	32	92	109
	SD.	1	3	2	16	12	7	6	6	15
STANDI	M01	-1	-3	-3	447	43	49	13	99	113
	M02	0	-3	0	487	47	20	13	93	135
	M03	-1	-2	4	469	44	48	6	98	107
	M04	-1	-2	2	451	27	33	18	88	89
	M05	1	-2	1	462	59	59	14	91	133
	M06	-1	-4	1	466	27	25	21	84	108
	F01	-2	-4	2	475	53	50	8	97	118
	F02	1	-3	2	468	57	37	17	90	120
	F03	-2	-5	-1	433	37	41	12	89	109
	AV.	-1	-3	1	462	44	40	14	92	115
	SD.	1	1	2	16	12	13	5	5	14
FWFLEX	M01	-2	52	-1	440	43	8	49	95	118
	M02	0	46	0	n/a	n/a	6	31	n/a	n/a
	M03	-3	41	7	472	45	27	40	89	115
	M04	-2	48	6	450	23	11	51	87	102
	M05	-1	49	0	460	48	21	48	89	135
	M06	-2	56	4	475	22	2	51	77	105
	F01	-4	58	6	484	58	33	40	92	119
	F02	-1	49	3	467	43	8	42	86	117
	F03	-2	47	2	429	20	37	13	89	97
	AV.	-2	50	3	460	38	17	40	88	113
	SD.	1	5	3	19	14	13	12	5	19

Appendix Table B: Volume for all deformable objects.

		Liver (cm^3)	KidneyL (cm^3)	KidneyR (cm^3)	Spleen (cm^3)	Abdomen (cm^3)	Thorax (cm^3)	Skin (cm^3)
SUPINE	M01	1473	155	137	167	4853	3993	24193
	M02	1744	173	190	284	6645	4961	32789
	M03	1358	137	131	116	4429	4442	21868
	M04	1593	129	139	124	4921	3920	21978
	M05	1667	151	143	418	5539	4601	26416
	M06	1461	154	190	171	7086	4099	33977
	F01	1701	165	140	159	4857	5220	22128
	F02	1759	190	134	133	4532	4026	20230
	F03	1521	131	139	128	5378	3149	19008
	AV.	1586	154	149	189	5360	4268	24732
	SD.	141	20	23	100	930	619	5352
SEATED	M01	1357	136	116	205	4566	4756	22855
	M02	1747	175	172	327	6524	6837	33849
	M03	1343	154	132	128	4214	5447	23346
	M04	1620	139	148	133	5045	4483	23922
	M05	1848	145	139	388	5855	5269	28094
	M06	1531	151	160	176	7171	4605	33829
	F01	1674	160	147	155	5090	5753	22602
	F02	1458	164	135	117	4839	4792	21878
	F03	1534	119	131	120	5386	5110	21206
	AV.	1568	149	142	194	5410	5228	25731
	SD.	171	17	17	98	952	732	4993
STANDI	M01	1358	135	117	190	4563	4937	24326
	M02	1682	151	173	287	6448	6793	34194
	M03	1271	152	131	119	4461	5680	23713
	M04	1523	134	151	138	5203	4805	24042
	M05	1787	159	142	419	5705	5126	27851
	M06	1531	154	165	175	7617	4533	35043
	F01	1504	130	144	139	5187	6107	22684
	F02	1356	193	153	131	4877	4746	22330
	F03	1394	130	129	126	5355	4711	20998
	AV.	1490	149	145	191	5491	5271	26131
	SD.	166	20	18	100	998	764	5167
FWFLEX	M01	1298	136	119	185	4344	5606	24111
	M02	1784	185	181	334	6544	n/a	n/a
	M03	1235	141	118	119	4038	6393	22560
	M04	1547	133	129	137	4807	5217	23229
	M05	1861	150	140	381	5768	5569	27916
	M06	1497	155	166	192	7009	4629	32478
	F01	1562	141	118	148	4656	6199	22574
	F02	1343	175	169	131	4685	5430	21443
	F03	1417	116	130	98	5375	4856	20940
	AV.	1505	148	141	192	5248	5487	24406
	SD.	212	21	25	99	1013	605	3904

Appendix Table C: Position of the center of the object in the spinal frame (in mm).

		Liver			KidneyL			KidneyR			Spleen			Abdomen			Thorax			Pelvis			Skin		
		X	Y	Z	X	Y	Z	X	Y	Z	X	Y	Z	X	Y	Z	X	Y	Z	X	Y	Z	X	Y	Z
SUPINE	M01	30	-61	196	-18	58	160	-2	-61	133	-23	97	191	31	-3	107	7	7	308	11	2	218	-5	-5	-50
	M02	14	-76	240	-36	65	175	-32	-67	165	-15	104	226	26	-8	141	5	8	340	11	0	228	-8	0	-56
	M03	26	-66	198	-2	56	136	-13	-65	139	-10	95	185	35	-11	120	9	1	314	7	-3	236	-4	1	-52
	M04	27	-62	198	-17	58	132	-17	-70	126	-26	79	188	33	-6	135	13	1	315	11	-1	231	2	3	-47
	M05	38	-59	196	5	70	131	6	-62	118	4	95	187	48	2	132	6	5	310	13	3	225	-1	3	-54
	M06	26	-66	246	-4	77	156	-5	-66	153	-16	82	242	50	-2	151	18	-5	360	29	-1	234	5	-2	-47
	F01	23	-56	179	-27	49	167	-8	-69	102	-1	86	197	25	-6	103	4	1	324	4	-4	237	-6	0	-55
	F02	16	-42	167	-40	63	143	-39	-49	131	-41	83	200	15	1	107	-2	6	313	-4	4	227	-7	9	-67
	F03	23	-66	194	-14	59	142	-2	-61	115	-24	84	190	52	-9	80	14	-1	302	14	-2	206	-6	-5	-52
	AV.	25	-62	202	-17	62	149	-12	-63	131	-17	89	201	35	-5	120	8	2	321	11	0	227	-3	1	-53
	SD.	7	9	26	15	8	16	15	6	19	14	8	20	13	4	22	6	4	18	9	3	10	4	4	6
SEATED	M01	20	-57	156	-26	63	143	-1	-62	106	-18	101	164	38	-5	77	-6	-1	293	1	-3	220	23	-4	-46
	M02	9	-62	177	-41	76	146	-51	-65	159	-14	114	179	37	-3	88	-18	3	311	-1	-2	230	12	-2	-55
	M03	41	-50	149	10	61	108	8	-73	96	18	96	144	55	-8	74	-4	3	294	4	-2	238	18	-2	-49
	M04	29	-49	176	-16	67	112	-7	-71	102	-26	87	171	44	-1	108	3	4	306	9	1	232	19	-1	-45
	M05	20	-53	179	-5	73	118	16	-63	89	-17	93	174	45	0	115	-13	7	308	2	2	228	25	-1	-47
	M06	40	-65	219	25	72	122	37	-74	110	-14	76	208	67	-5	128	17	-4	344	37	-3	224	12	-3	-46
	F01	9	-57	140	-32	59	128	9	-69	42	-6	91	153	34	-6	62	-12	1	300	-10	-3	233	28	-1	-50
	F02	17	-40	156	-34	66	119	-33	-63	115	-45	62	184	36	-5	77	-22	-5	306	-11	-5	224	26	0	-55
	F03	40	-68	155	-7	50	122	20	-66	89	-14	80	164	43	-9	84	13	-9	285	17	-10	217	15	-7	-47
	AV.	25	-56	167	-14	65	124	0	-67	101	-15	89	171	44	-5	90	-5	0	305	5	-3	227	20	-2	-49
	SD.	13	9	24	22	8	13	27	4	30	17	15	19	11	3	22	14	5	17	15	4	7	6	2	4
STANDI	M01	38	-49	138	-12	67	119	18	-54	86	-2	105	139	44	-1	50	-6	0	278	9	-2	207	1	-4	-50
	M02	9	-62	180	-47	66	153	-53	-66	155	-17	111	177	33	-3	82	-16	4	310	1	0	229	1	-2	-56
	M03	29	-50	160	1	61	126	-10	-64	127	1	101	148	41	-8	65	-7	1	296	2	-3	227	-4	1	-52
	M04	23	-55	171	-11	61	108	-7	-71	99	-28	81	166	39	-4	94	-6	-2	299	7	-5	222	4	3	-47
	M05	27	-48	173	14	74	101	34	-58	80	-4	95	160	47	2	90	-13	6	294	9	1	211	3	-3	-53
	M06	29	-63	207	8	73	114	20	-64	105	-26	81	199	58	-3	109	8	-5	331	30	-4	222	10	-4	-46
	F01	27	-52	135	-14	55	124	21	-67	39	9	93	149	36	-4	37	-11	0	297	4	-5	214	-1	2	-55
	F02	25	-37	148	-23	66	113	-27	-63	114	-36	65	174	35	-6	57	-21	0	299	-4	-1	212	4	-1	-55
	F03	26	-66	150	-5	54	109	24	-58	78	-30	78	151	27	-10	68	1	-9	275	10	-12	205	2	-4	-49
	AV.	26	-54	162	-10	64	119	2	-63	98	-15	90	163	40	-4	72	-8	-1	298	7	-3	217	2	-1	-51
	SD.	8	9	23	18	7	15	29	5	33	16	15	19	9	4	23	9	5	16	10	4	9	4	3	4
FWFLEX	M01	23	-42	142	-31	65	124	-4	-53	94	-11	96	147	42	-2	63	-16	2	279	-5	-1	225	32	-3	-41
	M02	19	-60	176	-39	71	142	-44	-67	146	0	107	183	41	-3	96	n/a	n/a	n/a	n/a	n/a	n/a	19	-2	-54
	M03	16	-43	159	-12	60	122	-17	-64	107	-4	102	149	40	-5	86	-14	6	298	-6	2	241	28	-1	-46
	M04	32	-45	158	-14	65	103	-25	-62	98	-11	92	149	48	-3	101	-3	5	289	1	0	235	31	3	-40
	M05	39	-49	171	6	67	104	17	-61	83	-7	86	162	55	0	114	-12	-3	299	11	-1	229	32	-2	-44
	M06	32	-55	222	7	69	119	-6	-49	132	-26	88	194	55	3	143	3	-4	341	23	-1	237	33	-4	-38
	F01	17	-53	146	-20	52	126	26	-67	52	2	88	158	44	-9	71	-25	2	301	-9	-4	231	30	1	-49
	F02	26	-31	148	-18	64	101	-32	-55	114	-39	66	170	43	-3	71	-15	0	299	-5	-2	227	28	-2	-50
	F03	61	-54	147	31	50	90	37	-49	72	7	70	146	50	-1	79	18	-9	278	22	-5	209	3	7	-50
	AV.	29	-48	163	-10	62	114	-5	-59	100	-10	88	162	46	-3	92	-8	0	298	4	-2	229	26	0	-46
	SD.	14	9	25	21	7	16	27	7	29	14	14	17	6	3	25	14	5	20	13	2	10	10	3	5

Appendix Table D: Inertial matrices of the solid organs in the axis of spinal frame and moved at the center of the organ.

		Liver (10^8 mm^4)						KidneyL (10^8 mm^4)						KidneyR (10^8 mm^4)						Spleen (10^8 mm^4)					
		Ixx	Iyy	Izz	Ixy	Ixz	Iyz	Ixx	Iyy	Izz	Ixy	Ixz	Iyz	Ixx	Iyy	Izz	Ixy	Ixz	Iyz	Ixx	Iyy	Izz	Ixy	Ixz	Iyz
SUPINE	M01	45.2	32.8	42.3	-8.9	0.6	-4	1.1	1.1	0.6	0.1	0.1	0.2	1.1	0.9	0.5	0	0.1	-0.3	1.3	1.2	0.8	-0.2	0	0.3
	M02	49.9	42.4	60.6	-7.8	-0.3	-5.1	1.6	1.4	0.7	0.1	0.1	0.3	1.6	1.5	0.9	-0.1	0.1	-0.4	2.3	2.7	2.3	-0.5	0.1	0.5
	M03	39	30.5	39.7	-8.5	0.3	-5.9	1.3	1.3	0.5	0	0.3	0.3	0.9	1	0.5	0	0.2	-0.2	0.7	0.7	0.4	-0.1	0	0.1
	M04	49.5	36.6	51.8	-11.1	-0.6	-8.1	0.9	0.8	0.4	0.1	0	0.2	1	1	0.5	-0.1	0.1	-0.2	0.8	0.5	0.6	-0.1	0	0.1
	M05	40.8	43	50.3	-7.8	-2.8	-7.8	1.1	1	0.6	0	0.1	0.2	1	1.1	0.6	0	0.2	-0.2	4.3	5.6	5.7	-1.3	0.7	0.6
	M06	33.3	31.8	43	-5.2	-3.2	-5.5	1.1	1.1	0.5	0	0.1	0.2	1.6	1.5	0.8	0	0.2	-0.3	1.3	1.1	1	-0.3	0.1	0.2
	F01	53.5	43.8	53.7	-12.4	5.4	-1.3	1.4	1.3	0.6	0.1	0.1	0.2	0.9	0.8	0.5	-0.1	0.1	-0.1	0.8	0.9	1.1	0	0.1	0.2
	F02	69.9	66.7	43.1	-12.4	6.2	1.8	1.8	1.7	0.7	0.1	0.1	0.3	1.3	1.3	0.4	0	0.2	-0.2	0.9	0.7	0.7	-0.1	0.1	0.3
	F03	39.9	38.6	38.1	-5.4	-0.9	-6.9	0.9	0.8	0.5	0	0.1	0.2	1	1.1	0.5	0	0.2	-0.2	0.8	0.7	0.5	-0.1	0.1	0.1
	AV.	46.8	40.7	46.9	-8.8	0.5	-4.8	1.2	1.2	0.6	0	0.1	0.3	1.2	1.1	0.6	0	0.2	-0.2	1.5	1.6	1.5	-0.3	0.1	0.3
	SD.	10.7	10.9	7.5	2.7	3.3	3.2	0.3	0.3	0.1	0.1	0.1	0.1	0.3	0.2	0.2	0	0.1	0.1	1.2	1.6	1.7	0.4	0.2	0.2
SEATED	M01	43.1	29.3	38.3	-8.8	4	-1.2	0.9	0.9	0.5	0	0.2	0.2	0.8	0.9	0.4	0	0.3	-0.2	1.7	2.1	1.3	-0.3	0.4	0.4
	M02	59.4	44.2	57.8	-12.8	5.9	-2.5	1.4	1.4	0.8	0	0.3	0.3	1.3	1.2	0.8	0	0.2	-0.4	2.8	3.9	2.8	-0.4	0.5	0.4
	M03	41	32.7	41.5	-11.2	6.1	-2.6	1.5	1.5	0.6	-0.1	0.4	0.3	0.9	1.1	0.5	0	0.3	-0.1	0.8	1	0.6	-0.1	0.2	0.1
	M04	50.1	36.7	54.8	-12.6	1.8	-6.1	1	1	0.5	0	0.1	0.2	1	1.2	0.7	-0.1	0.4	-0.1	0.9	0.7	0.7	-0.1	0.1	0.1
	M05	49.9	49.1	61.8	-12	1.7	-7.5	0.9	1	0.6	-0.1	0.3	0.2	0.8	1.1	0.7	-0.1	0.4	0	4	5.7	5.2	-1.2	1	0.6
	M06	35.8	37.1	44.5	-8	-3.3	-6.6	1.1	1.2	0.5	0	0.2	0.1	1.1	1.3	0.7	0	0.4	-0.1	1.4	1.1	1	-0.3	0.2	0.2
	F01	59.4	51.1	50.8	-12.1	7.9	-0.1	1.3	1.3	0.6	0.1	0.3	0.1	0.7	1	0.9	-0.1	0.3	-0.1	0.7	1.4	0.9	0	0.3	0.1
	F02	49.1	38.5	40.5	-10.4	6.8	-1.3	1.4	1.5	0.7	-0.1	0.4	0.2	1.2	1.2	0.5	0	0.4	-0.1	0.7	0.4	0.7	-0.1	0	0.1
	F03	44.6	37.6	40.8	-6.5	1.2	-7.5	0.9	0.8	0.4	0	0.1	0.2	0.8	1.2	0.6	0	0.4	-0.1	0.8	0.6	0.6	-0.2	0.1	0.1
	AV.	48	39.6	47.9	-10.5	3.6	-3.9	1.2	1.2	0.6	0	0.3	0.2	1	1.1	0.6	0	0.3	-0.1	1.5	1.9	1.5	-0.3	0.3	0.2
	SD.	7.9	7.2	8.6	2.2	3.5	3	0.2	0.3	0.1	0	0.1	0.1	0.2	0.1	0.2	0	0.1	0.1	1.2	1.8	1.5	0.4	0.3	0.2
STANDI	M01	46.3	29.7	39	-8	4.3	-2.7	0.9	0.9	0.5	0	0.2	0.2	0.8	0.9	0.5	0	0.3	-0.1	1.6	1.8	1	-0.2	0.3	0.3
	M02	54.2	40.2	54.4	-12.6	4.7	-1.6	1.2	1.2	0.6	0	0.2	0.2	1.3	1.3	0.8	0	0.2	-0.3	2.3	3.3	2.3	-0.4	0.4	0.4
	M03	39	30.4	39.3	-10.5	5.9	-1.6	1.3	1.4	0.7	-0.1	0.5	0.3	0.9	1.1	0.6	0	0.3	-0.2	0.7	0.9	0.6	-0.1	0.2	0
	M04	45	32.9	50.9	-11.5	1.4	-5.7	0.9	1	0.5	0	0.2	0.2	0.9	1.3	0.7	-0.1	0.4	0	0.9	0.7	0.8	-0.2	0	0
	M05	46.8	47.9	60.3	-13.1	1.5	-5.6	1.1	1.2	0.7	0	0.3	0.2	0.9	1.2	0.7	-0.1	0.4	0	4.1	6.6	6	-1.2	1.1	0.5
	M06	34.6	38	45.2	-7.4	-2.9	-6	1	1.2	0.6	0	0.3	0.1	1.1	1.5	0.9	0	0.5	-0.1	1.4	1.5	1	-0.3	0.3	0.2
	F01	50.4	45.5	42.9	-12.2	8.2	2.2	0.9	0.9	0.4	0	0.2	0.1	0.8	1	0.7	-0.1	0.3	0	0.6	1	0.7	-0.1	0.2	0.1
	F02	46.4	40.4	36.9	-9.1	7.7	-4.6	1.6	1.8	0.9	-0.1	0.5	0.2	1.4	1.6	0.7	0.1	0.6	-0.2	0.8	0.5	0.8	-0.1	0	0.2
	F03	37.1	33.1	36.2	-6	2.1	-6	0.8	0.8	0.6	-0.1	0.2	0.2	0.8	1.1	0.6	-0.1	0.4	0	0.8	0.7	0.7	-0.2	0.2	0.1
	AV.	44.4	37.5	45	-10.1	3.7	-3.5	1.1	1.2	0.6	0	0.3	0.2	1	1.2	0.7	0	0.4	-0.1	1.5	1.9	1.5	-0.3	0.3	0.2
	SD.	6.4	6.5	8.4	2.5	3.5	2.8	0.3	0.3	0.2	0	0.1	0.1	0.2	0.2	0.1	0	0.1	0.1	1.1	2	1.7	0.4	0.3	0.1
FWFLEX	M01	43.9	26.1	38.1	-7	3.5	-3.4	0.9	0.9	0.5	0	0.2	0.2	0.7	0.9	0.5	0	0.3	-0.1	1.4	1.8	1	-0.1	0.2	0.2
	M02	58.1	47.3	57.6	-13.5	4.5	-4.7	1.5	1.6	0.9	0	0.4	0.2	1.4	1.5	0.9	0	0.3	-0.4	2.7	3.9	3	-0.5	0.4	0.4
	M03	34.8	25.6	37.6	-9.2	3.2	-4	1.3	1.3	0.6	-0.1	0.4	0.3	0.6	0.9	0.5	0	0.3	-0.1	0.6	0.8	0.5	-0.1	0.1	0.1
	M04	45.4	38.6	49.9	-12.4	1.3	-7.8	0.9	1	0.5	0	0.3	0.2	0.7	0.9	0.5	0	0.2	-0.1	0.7	0.9	0.8	-0.2	0.1	0
	M05	52.7	50.7	61.9	-13.2	0	-9.2	1	1.1	0.7	0	0.3	0.2	0.8	1.1	0.7	-0.1	0.4	0	3.3	5	4.9	-1	0.8	0.4
	M06	33.2	35.7	44.2	-7.2	-3.4	-6.3	1	1.3	0.6	0	0.4	0	1.1	1.4	0.8	0	0.4	-0.1	1.4	1.5	1.4	-0.4	0.3	0.2
	F01	54.1	46.3	42.2	-9.2	8.6	-3.1	1	1.2	0.6	0	0.3	0.1	0.5	0.8	0.6	0.1	0.2	-0.1	0.6	1.1	0.8	-0.1	0.2	0.1
	F02	43.2	36.5	34.2	-8.6	6	-3.5	1.4	1.5	0.9	0	0.5	0.2	1.5	1.7	0.8	0	0.6	-0.2	0.8	0.5	0.8	-0.1	0	0.2
	F03	38.8	34.7	32.7	-6.2	0.6	-6	0.7	0.8	0.4	0	0.2	0.1	0.9	1.1	0.5	-0.1	0.3	0.1	0.5	0.4	0.5	-0.1	0.1	0
	AV.	44.9	37.9	44.2	-9.6	2.7	-5.3	1.1	1.2	0.6	0	0.3	0.2	0.9	1.1	0.7	0	0.3	-0.1	1.3	1.8	1.5	-0.3	0.3	0.2
	SD.	8.6	8.9	10.3	2.8	3.5	2.1	0.2	0.3	0.2	0	0.1	0.1	0.4	0.3	0.1	0.1	0.1	0.1	1	1.6	1.5	0.3	0.3	0.2

Appendix Table E: Inertial matrices of the large objects in the axis of spinal frame and moved at the center of the object. In 10^8 mm^4.

		Abdomen						Thorax						Skin					
		Ixx	Iyy	Izz	Ixy	Ixz	Iyz	Ixx	Iyy	Izz	Ixy	Ixz	Iyz	Ixx	Iyy	Izz	Ixy	Ixz	Iyz
SUPINE	M01	748	581	267	7	-5	34	245	147	215	0	12	13	6324	4877	2742	96	532	-87
	M02	1098	804	452	-8	30	74	360	204	326	-5	14	22	11122	9213	4338	31	1297	-36
	M03	562	417	239	-16	7	29	331	178	262	-13	14	14	5700	4584	2138	-89	518	8
	M04	578	410	277	-7	25	19	258	135	223	-8	9	3	5329	4098	2249	-84	262	-51
	M05	655	493	313	-9	10	9	298	173	272	-11	9	3	6603	5325	3045	-83	679	-2
	M06	960	737	419	-17	59	33	265	154	224	-10	13	2	10194	8355	4346	-93	613	186
	F01	643	467	270	-5	24	39	381	254	282	-3	16	9	6228	5202	2081	-33	578	74
	F02	624	518	203	-10	20	30	250	146	209	-7	15	0	4494	3690	1817	-55	349	95
	F03	622	493	252	-7	19	12	171	94	160	-5	9	3	4742	3807	1708	-38	395	14
	AV.	721	547	299	-8	21	31	284	165	241	-7	12	8	6748	5461	2718	-39	580	22
	SD.	186	138	83	7	18	19	66	45	49	4	3	7	2337	1980	1011	64	300	84
SEATED	M01	540	420	248	2	83	19	330	213	243	0	15	6	5392	4322	2394	46	470	-23
	M02	839	660	424	-18	138	33	592	366	475	-18	11	30	9530	7807	4703	-63	882	52
	M03	427	341	195	-18	41	18	482	287	323	-18	26	10	6092	4807	2578	-110	612	-30
	M04	502	383	257	-5	66	11	335	186	255	-14	13	4	6027	4712	2643	-96	361	-30
	M05	585	474	345	-11	104	5	381	235	309	-14	13	6	6882	5617	3459	-77	610	28
	M06	891	730	404	-9	76	16	320	193	256	-6	17	0	9973	8594	4303	-55	1090	66
	F01	583	463	300	-23	109	54	462	310	318	-10	10	13	5655	4652	2260	-70	498	11
	F02	509	465	214	-9	106	24	336	208	251	-6	5	-1	4941	4158	2109	-26	549	82
	F03	624	495	252	2	20	13	366	226	290	0	11	1	4864	3826	2100	9	356	-8
	AV.	611	492	293	-10	83	21	400	247	302	-10	13	8	6595	5388	2950	-49	603	16
	SD.	155	126	81	9	37	15	93	61	72	7	6	10	1896	1681	975	50	241	43
STANDI	M01	558	443	222	2	27	15	355	241	251	5	13	8	6261	5036	2773	83	696	16
	M02	905	727	396	-18	114	38	579	362	472	-18	11	26	10144	8233	4820	-105	1042	38
	M03	555	458	210	-16	34	23	472	281	343	-18	12	12	6508	5201	2627	-102	702	85
	M04	592	486	262	-10	76	15	359	203	282	-10	2	3	6018	4719	2740	-73	491	52
	M05	682	587	305	-10	70	-6	357	218	304	-15	11	7	7064	5782	3471	-41	890	40
	M06	980	832	448	-5	95	18	312	190	248	-5	14	2	10260	8592	4862	38	998	128
	F01	652	539	251	-20	35	51	492	348	335	-5	12	7	6069	5200	2229	-54	794	120
	F02	566	519	195	-2	61	2	323	207	239	-9	5	-3	5275	4580	2228	-66	782	17
	F03	627	496	252	0	7	20	318	196	258	-2	1	0	4773	3770	2095	4	411	113
	AV.	680	565	282	-9	58	20	396	249	304	-9	9	7	6930	5679	3094	-35	756	67
	SD.	156	132	86	8	35	17	94	66	74	8	5	8	1969	1646	1072	64	211	45
FWFLEX	M01	445	365	206	4	77	10	443	278	325	7	2	2	5593	4224	2882	75	225	56
	M02	784	612	389	-17	103	27	n/a	n/a	n/a	n/a	n/a	n/a	n/a	n/a	n/a	n/a	n/a	n/a
	M03	381	305	192	-16	58	4	569	351	392	-17	-2	10	5351	4226	2360	-73	349	-45
	M04	394	317	232	-10	61	-3	408	248	303	-18	-5	-1	5361	4191	2554	-132	293	16
	M05	520	429	309	-8	79	7	411	253	336	2	0	-1	6525	5272	3481	18	287	-5
	M06	725	589	388	-2	81	-4	328	199	257	-4	5	-2	8355	7231	4139	-45	392	163
	F01	464	375	254	-19	90	29	490	352	347	-14	2	11	5361	4624	2237	-44	630	5
	F02	448	418	197	1	85	-1	398	268	289	-15	3	-3	4729	4084	1976	-60	414	25
	F03	624	494	252	-1	11	20	340	213	262	-1	13	-4	4778	4022	1974	5	563	24
	AV.	532	434	269	-8	72	10	423	270	314	-8	2	1	5757	4734	2700	-32	394	30
	SD.	146	111	77	8	27	13	79	57	46	10	5	6	1187	1087	767	63	140	61